Fe-based superconducting thin films on metallic substrates: Growth, characteristics, and relevant properties

Kazumasa Iida, Jens Hänisch, and Chiara Tarantini

Articles you may be interested in

The influence of the in-plane lattice constant on the superconducting transition temperature of $FeSe_{0.7}Te_{0.3}$ thin films
AIP Advances **7**, 065015 (2017); 10.1063/1.4989566

A practical field guide to thermoelectrics: Fundamentals, synthesis, and characterization
Applied Physics Reviews **5**, 021303 (2018); 10.1063/1.5021094

Fundamentals and applications of optomechanically induced transparency
Applied Physics Reviews **5**, 031305 (2018); 10.1063/1.5027122

Plasma physics of liquids—A focused review
Applied Physics Reviews **5**, 031103 (2018); 10.1063/1.5020511

Chip-scale atomic devices
Applied Physics Reviews **5**, 031302 (2018); 10.1063/1.5026238

Harvest of ocean energy by triboelectric generator technology
Applied Physics Reviews **5**, 031303 (2018); 10.1063/1.5008606

APPLIED PHYSICS REVIEWS

Fe-based superconducting thin films on metallic substrates: Growth, characteristics, and relevant properties

Kazumasa Iida,[1,a)] Jens Hänisch,[2] and Chiara Tarantini[3]

[1]*Department of Materials Physics, Nagoya University, Furo-cho, Chikusa-ku, Nagoya 464-8603, Japan*
[2]*Institute for Technical Physics, Karlsruhe Institute of Technology, Hermann-von-Helmholtz-Platz 1, D-76344 Eggenstein-Leopoldshafen, Germany*
[3]*Applied Superconductivity Center, National High Field Laboratory, Florida State University, Tallahassee, Florida 32310, USA*

The discovery of Fe-based superconductors (FBS) as the second class of high-temperature superconducting transition (high-T_c) materials after the cuprates generated a significant impact on the community of fundamental and applied superconductivity research. Whenever a new class of high-T_c superconducting materials is discovered, a lot of effort is devoted to growing single crystals and epitaxial thin films for exploring basic physical quantities. Although several properties of FBS are similar to the cuprates (large upper critical fields, as a consequence short coherence lengths and small carrier density), others are distinctly different. For instance, in FBS, the symmetry of the superconducting order parameter is most likely not a d-wave but an $s\pm$-wave, depending on the stoichiometry, crystallographic system, and doping level. Additionally, the critical current densities of FBS are less sensitive to the presence of grain boundaries (GBs) than those of the high-T_c cuprates. These features are highly beneficial for the realization of cheaper conductors for high-field magnets at low temperatures. Indeed, several groups have demonstrated FBS thin films on technical metallic substrates and powder-in-tube processed FBS wires as proof-of-principle studies for conductor applications. FBS on technical substrates also give many opportunities for studying how GB networks affect the critical current and how uniaxial strain impacts the superconducting properties. In this article, we review FBS thin films, especially on technical metallic substrates, and focus on application-relevant properties like pinning improvement by natural and artificial defects as well as the transparency of grain boundaries and GB networks. The recent development of FBS thin films on technical substrates and their superconducting properties are presented and the performance gap with respect to films on single crystals is discussed. *Published by AIP Publishing.* https://doi.org/10.1063/1.5032258

TABLE OF CONTENTS

I. INTRODUCTION

Since the first report of superconductivity in LaFeAs(O,F) 10 years ago by Hosono's group,[1] a lot of progress in the

a)Electronic mail: iida@mp.pse.nagoya-u.ac.jp

growth and synthesis of Fe-based superconducting (FBS) single crystals, bulks, wires, and thin films has been made. Now, high-quality thin films [e.g., FeSe, Fe(Se,Te), doped and undoped $AE\mathrm{Fe_2As_2}$, where AE being an alkali earth element, and $Ln\mathrm{FeAs(O,F)}$, where Ln is a lanthanoide element, named, respectively, 11, 122, and 1111] are available on a large variety of single-crystalline and technical substrates. Hence, fundamental as well as application-oriented research has been remarkably developed. In this article, we review FBS thin films, especially on technical metallic substrates, and focus on application-related properties like pinning improvement by natural and artificial defects as well as the transparency of grain boundaries (GBs) and GB networks. Many excellent review articles focussing on the growth of FBS thin films on single crystals and their physical properties have already been published[2–9] and the interested readers may also refer to them. The structure of this article is as follows: Naturally grown pinning centers are summarized, followed by artificial pinning centers. Afterwards, grain boundary experiments on Fe(Se,Te), doped $\mathrm{BaFe_2As_2}$ (Ba-122), and NdFeAs(O,F) will be reviewed. Finally, FBS thin films on technical substrates will be described and discussed.

II. PINNING IMPROVEMENTS

One of the most important properties for wire and tape applications is the critical current density J_c, which can be improved by microstructural engineering. Similar to the high-T_c cuprates, the coherence length of FBS is on the order of a few nm.[17] Hence nano-sized precipitates and defects can strongly pin the vortices in the mixed state. When transport currents flow in FBS in the mixed state, the Lorentz force acts on the vortices. If the pinning force is weaker than the Lorentz force, the vortices start to move, resulting in dissipation of energy. Hence, the stronger the pinning force density, the higher the critical current density. Another effect which depins vortices is thermal fluctuations. This is quantified by the Ginzburg number (Gi) defined as the ratio of the minimal condensation energy within the coherence volume and the thermal energy at the critical temperature ($k_B T_c$, where k_B is the Boltzmann constant). Thermal fluctuations are a serious problem for high-T_c superconductors (HTS), for instance, in $\mathrm{YBa_2Cu_3O_7}$ (YBCO) with a high Gi of around 10^{-3} (Table I). For anisotropic superconductors, Gi number in SI (International System) unit is evaluated by the following equation:[18]

$$Gi = \frac{1}{2}\left(\frac{k_B T_c}{4\pi\mu_0 H_c^2(0)\epsilon\xi^3(0)}\right)^2 = \frac{\pi\mu_0^2 k_B^2}{\phi_0^3}\frac{\kappa^4 T_c^2}{\mu_0 H_{c2}(0)\epsilon^2}$$
$$= 1.07 \times 10^{-13}\frac{\kappa^4 T_c^2}{\mu_0 H_{c2}(0)\epsilon^2}, \qquad (1)$$

where $\mu_0 H_c(0) = \mu_0 H_{c2}(0)/\sqrt{2}\kappa$ is the thermodynamic critical field at 0 K, $\mu_0 H_{c2}(0)$ is the upper critical field in c-direction at 0 K, ϵ is the anisotropy parameter defined as $\xi_c(0)/\xi_{ab}(0)$, $\xi_{ab}(0) = \sqrt{\frac{\phi_0}{2\pi\mu_0 H_{c2}(0)}}$ is the in-plane coherence length at 0 K, κ is the Ginzburg-Landau parameter at 0 K, and the right hand side is valid for basic SI units. It is noted that the $\mu_0 H_{c2}(0)$ is calculated by using the Werthamer-Helfand-Hohenberg (WHH) formula. By using Eq. (1), Gi for various FBS is evaluated (Table I). Only for 122 and FeSe, Gi is smaller than for YBCO and, therefore, the flux creep at the probable operating temperatures (minimum flux creep rate is expressed by $S \sim Gi^{1/2}(T/T_c)$ due to thermal fluctuations is not a serious problem).[19] Different is the case of the most anisotropic NdFeAs(O,F) and Fe(Se,Te) that could more strongly suffer from thermal fluctuations.

In general, thin films contain a higher density of natural defects than single crystals. In low magnetic fields, J_c for thin films is higher than for single crystals (Fig. 1), whereas in high fields they appear to merge toward similar values. It is also noted that for single crystals, J_c has a non-monotonic field dependence due to the fish tail effect, whereas such an effect is absent in thin films. Considering the good performance already obtained in clean thin films, improvements in the in-field behavior are achievable by the introduction of artificial pinning centers with an appropriate control of their dimensionality (1D: columnar defects and dislocations, 2D: grain boundaries and anti-phase boundaries, and 3D: particles[27]) and their density.

In this section, the naturally grown pinning centers and artificial pinning centers in FBS are reviewed, and how these pinning centers influence the in-field J_c is discussed.

A. Naturally grown pinning centers

1. Ba-Fe-O nanopillars

Lee *et al.* implemented $\mathrm{SrTiO_3}$ as buffer layer to grow epitaxial Co-doped Ba-122 on 001-oriented substrates

TABLE I. Summary of Gi for various FBS calculated by Eq. (1) together with the physical quantities used for the calculations. The minimum flux creep rate S at the possible operating temperature T_{op} is also shown. For comparison, the data for YBCO and $\mathrm{MgB_2}$ are tabulated.

| Materials	T_c (K)	κ	ϵ	$\mu_0 H_{c2}$ (0) (T)	$Gi (\times 10^{-3})$	$S (\times 10^{-2})$ at T_{op}
FeSe[10]	8	72	0.55	16	0.04	0.3 at 4.2 K
Fe(Se$_{0.5}$Te$_{0.5}$)[11]	14	287	0.27	116	17.2	3.9 at 4.2 K
Co-doped Ba-122 (Ref. 12)	22	66	0.5	38	0.1	0.2 at 4.2 K
P-doped Ba-122 (Ref. 13)	29	93	0.4	49	0.9	0.4 at 4.2 K
K-doped Ba-122 (Ref. 10)	38	80	0.5	180	0.1	0.6 at 20 K
NdFeAs(O,F)[14]	35	113	0.13	60	20.6	8.2 at 20 K
NdFeAs(O,F)[15]	47	87	0.11	162	6.5	3.4 at 20 K
YBCO[10]	91	62	0.24	180	1.3	3.0 at 77 K
MgB$_2$ (Ref. 16)	38	8	0.23	3	4×10^{-3}	0.1 at 20 K
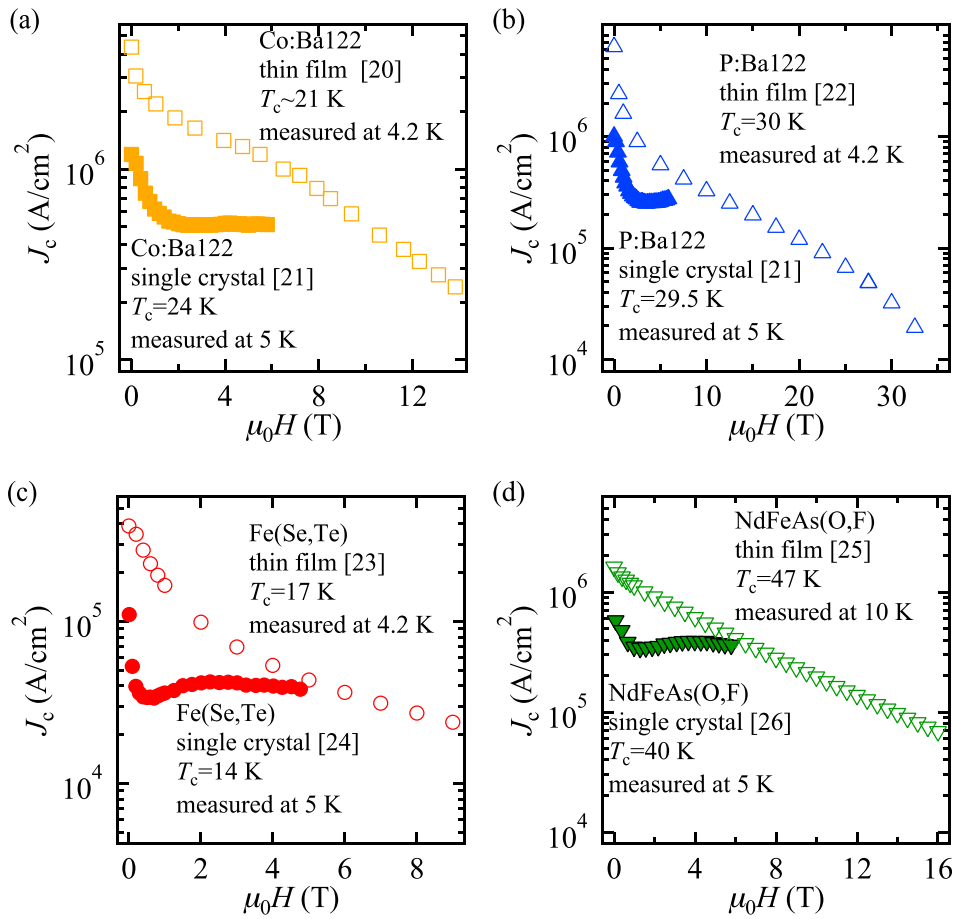
FIG. 1. Comparison of J_c-H properties between FBS thin films and single crystals. The applied magnetic field was $H \parallel c$ and the measurement temperatures are shown in figure: (a) Co-doped Ba-122 on 50 unit cell $BaTiO_3$-buffered $(LaAlO_3)_{0.3}(Sr_2TaAlO_6)_{0.7}$ prepared by pulsed laser deposition (PLD)[20] and optimally Co-doped Ba-122 single crystal.[21] (b) P-doped Ba-122 on MgO prepared by molecular beam epitaxy (MBE)[22] and optimally P-doped Ba-122 single crystal.[21] (c) Fe(Se,Te) on Fe-buffered MgO prepared by PLD[23] and $Fe_{1+y}Te_{0.6}Se_{0.4}$ single crystal.[24] (d) NdFeAs(O,F) on MgO fabricated by MBE[25] and single crystal.[26]

$[(LaAlO_3)_{0.3}(Sr_2TaAlO_6)_{0.7}$ (LSAT), $GdScO_3$, $LaAlO_3$, and Si] by pulsed laser deposition (PLD, KrF excimer laser).[20] The nominal Co doping level of their PLD target was $x = 0.08$ in $Ba(Fe_{1-x}Co_x)_2As_2$ with a small As excess to compensate the loss of As during the deposition. They concluded that the use of a $SrTiO_3$ template widened the range of possible substrates for high-quality Co-doped Ba-122 thin films. They also observed the formation of a high density of Ba-Fe-O nanopillars ($\sim$8 vol. %) that grew vertically from $SrTiO_3$ to the film surface (Fig. 2). As a result, the critical current density (J_c) for $H \parallel c$ was higher than that for $H \parallel ab$, which differs from what is expected by the mass anisotropy. The mean distance between nanopillars was 16–17 nm, which corresponds to a matching field of 7–8 T.[28] Indeed, the pinning force density showed a peak at

around 8 T for $H \parallel c$. Later, it was found that the oxygen content of the PLD targets strongly affects the Ba-Fe-O nanopillar density.[29] Most importantly, this compound can accept a high density of Ba-Fe-O of up to 20 vol. % without compromising T_c.

The detailed microstructural analysis by TEM identified the Ba-Fe-O phase as $BaFeO_2$, which is an isostructure of tetragonal $SrFeO_2$ ($a = 0.3991$ nm and $c = 0.3474$ nm).[30] The authors explained that $BaFeO_2$ has $a > 0.3991$ nm due to a larger ionic radius of Ba compared to Sr and is coherently strained by the Ba-122 matrix.

2. Threading dislocations

c-axis-correlated defects were also reported in Fe(Se,Te) thin films fabricated on $SrTiO_3$ (001) substrates by PLD (KrF excimer laser) in Genova. In Fig. 3, a high density of such defects with 2 nm diameter, comparable to the coherence length, was observed.[31] Bellingeri *et al.* speculated that those defects were threading dislocations. Owing to these defects, J_c for $H \parallel c$ was higher than for $H \parallel ab$ at all temperatures, which is similar to the observation reported for nanopillars in Co-doped Ba-122.[20] The mean defect separation was about 10 nm, corresponding to a matching field of 20 T. Consequently, J_c for $H \parallel c$ has a weaker field dependence than that for $H \parallel ab$ up to the maximum measured field of 9 T and in the temperature range below $0.65T_c$. The activation energy U_0 for vortex motion was raised by a factor

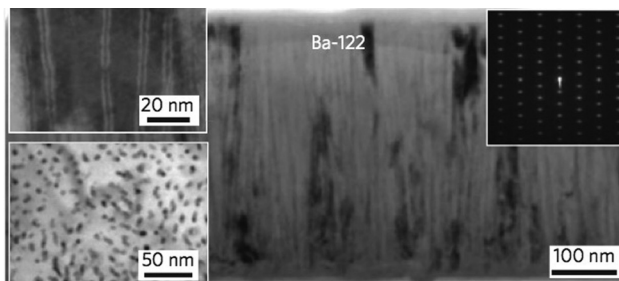

FIG. 2. Cross-sectional and planer view of TEM images of a Co-doped Ba-122 thin film fabricated on $SrTiO_3$-buffered LSAT(001). Reproduced with permission from Lee *et al.*, Nat. Mater. **9**, 397–402 (2010). Copyright 2010 Spring Nature.
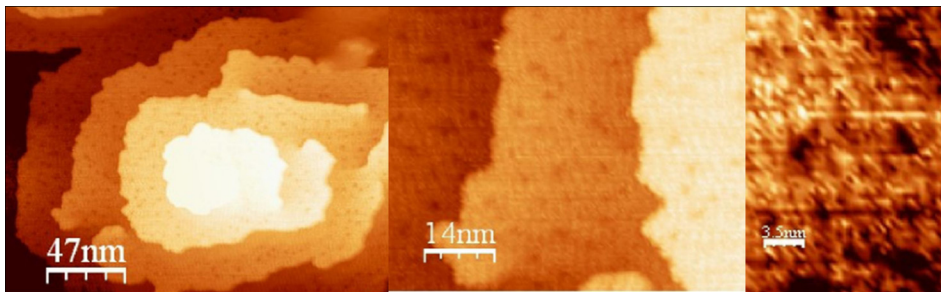
FIG. 3. Surface morphology of an Fe(Se,Te) film deposited by PLD on SrTiO₃(001) substrate investigated by STM. Reproduced with the permission from Appl. Phys. Lett. **100**, 082601 (2012). Copyright 2012 AIP Publishing LLC.

of 1.5 in these samples compared to a film on LaAlO₃(100) substrate, where interestingly this kind of defects was absent.

The introduction of threading dislocations in a controlled manner by tuning the growth conditions was reported for P-doped Ba-122 thin films by Sato *et al*.[32] Shown in Figs. 4(a) and 4(b) are the cross sectional views of two P-doped Ba-122 thin films grown on MgO substrates by PLD (Nd:YAG laser with 2nd harmonic) with different growth rates. Relatively short defects which are almost parallel to the Ba-122 c-axis were observed for a growth rate of 2.2 Å/s and identified as threading dislocations [Fig. 4(a)]. On the other hand, tilted, long defects of relatively low density were seen for the film grown at 3.9 Å/s and identified as domain boundaries due to lateral growth [Fig. 4(b)]. The film grown at 2.2 Å/s with threading dislocations showed the highest J_c in the full angular range among the films measured at 12 K and 3 T [Fig. 4(c)].

3. Fe precipitates

Hänisch *et al*. investigated Co-doped Ba-122 thin films containing 45° rotated grains grown by PLD (KrF excimer laser).[33] They fabricated Co-doped Ba-122 thin films on LSAT(001) at a relatively low deposition temperature of 675 °C in ultra-high vacuum (UHV) condition. As a result, round and c-axis elongated Fe precipitates were observed near or within the grain boundaries (Fig. 5). These Fe particles, together with the threading dislocations in the GBs, lead to a c-axis peak in the J_c anisotropy.

For P-doped Ba-122 thin films grown by molecular beam epitaxy (MBE), Sakagami *et al*. reported a maximum self-field J_c of 10 MA/cm² (4.2 K) for Fe-rich films (Fe/Ba = 2.4) on MgO(001) substrates measured by a magnetization method.[34] Although no microstructural investigations have been reported, the authors speculated two plausible reasons: one possibility is that nanoparticles of Fe or Fe-based compounds, which were not detectable by x-ray diffraction (XRD), are dispersed in the matrix of such Fe-rich P-doped Ba-122 films and act as pinning centers. The other possibility is that an Fe layer is formed at the interface with the substrate and acts as a buffer layer that improves the crystallinity.
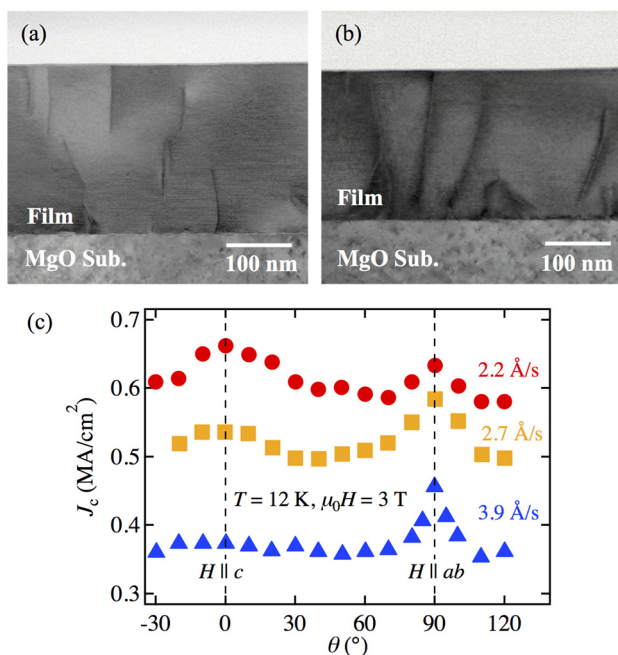

FIG. 4. Microstructure and J_c anisotropy of PLD-grown P-doped Ba122 films with intentional threading dislocations. Cross-sectional view of P-doped Ba-122 thin films grown at a rate of (a) 2.2 Å/s and (b) 3.9 Å/s. (c) Angular dependence of J_c of P-doped Ba-122 deposited at various growth rates measured at 12 K and 3 T. The figure is redrawn with some modifications based on the data taken from Fig. 2 in Ref. 32.
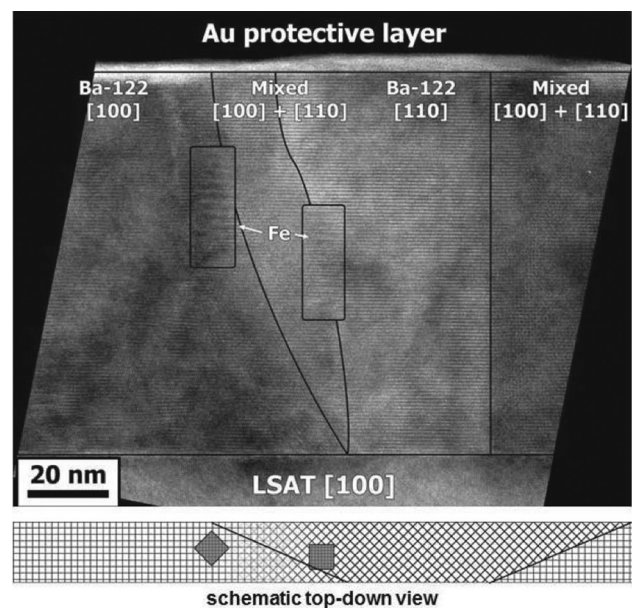

FIG. 5. Cross sectional TEM image of a PLD-grown Co-doped Ba-122 film on LSAT, revealing a sharp substrate-film interface, 45° [001] tilt GBs (vertical black lines) and round and c-axis elongated Fe precipitates (encircled) near or within the GBs. The image was taken in the (100) pole. The TEM image is a schematic top-down view illustrating the orientation of GBs and Fe particles, deduced from Moiré contrasts. Reproduced with permission from AIP Conf. Proc. **1574**, 260 (2014). Copyright 2014 AIP Publishing LLC.

B. Artificial pinning centers

1. BaZrO₃ nanoparticles in PLD-grown Co- and P-doped Ba-122

Using the same strategy for pinning enhancement of YBa₂Cu₃O₇ films,[35] BaZrO₃-added BaFe₂(As₁₋ₓPₓ)₂,[36] and Ba(Fe₁₋ₓCoₓ)₂As₂,[37] sintered pellets were prepared by two groups for use as PLD targets. The former target was ablated by a 2nd harmonic Nd:YAG laser, whereas the latter was ablated by a KrF excimer laser.

In P-doped Ba-122 films on MgO(001) substrate, nano-sized BaZrO₃ particles with average diameter of 5–10 nm were finely distributed in the Ba-122 matrix.[36] As a result, an almost isotropic J_c of 1.5 MA/cm² at 15 K ($0.6T_c$) and 1 T was obtained. In Co-doped Ba-122 films on CaF₂(001) substrate, short and c-axis-oriented BaZrO₃ nanorods with ∼4 nm diameter, slightly larger than in YBCO (2–3 nm),[41] were formed in the Ba-122 matrix.[37] The mean separation of BaZrO₃ nanorods was 10–11 nm, corresponding to a matching field of 17–20 T. The optimized Co-doped Ba-122 with 2 mol. % BaZrO₃ showed an in-field J_c of 1.3 MA/cm² at 13 T and 4.2 K.

Figure 6 compares the reduction of T_c in P-doped Ba-122 and Co-doped Ba-122. Up to 3 mol. % (2.5 vol. %) of BaZrO₃, the initial suppression rate of T_c for both films is around −1 K/mol. % (−1.3 K/vol. %), which is high compared to common values for GdBa₂Cu₃O₇ (GdBCO)[38] and YBCO.[39,40] The difference in T_c reduction against volume fraction is not as severe because of the smaller molar volume of the Ba-122 phase.

Compared to BaFeO₂ nanopillars (see section *Ba-Fe-O*), the reduction of T_c is significant, which may be ascribed to the different lattice mismatch.

2. Superlattices and multilayers

To date, FBS superlattices for Ba-122 (Ref. 42) and Fe(Se,Te)[43] have been reported by the Univ. Wisconsin and the Univ. of Tokyo, respectively. Lee *et al.* investigated the effect of SrTiO₃ and undoped Ba-122 insertion layers on the structural and superconducting properties of Co-doped Ba-122 thin films. The cross-sectional TEM images of the (100) projection clearly showed the 24 bilayers of SrTiO₃/Co-doped Ba-122 [Fig. 7(a)]. On the other hand, the insertion layer of undoped Ba-122 grew discontinuously in the lateral direction [Fig. 7(b)]. Similar to the single layer reported by the same group, the undoped oxygen-rich Ba-122/Co-doped Ba-122 superlattice possessed vertical defects, presumably BaFeO₂, which act as effective pinning centers along the crystallographic c-direction. Combining the c-axis and ab-planar pinning contributions improved in-field J_c properties considerably, as shown in Fig. 7(c).

Nabeshima *et al.* deposited FeSe/FeTe superlattices on CaF₂ and LaAlO₃.[43] From the microstructural investigations, some degree of Te/Se interdiffusion was observed. Because of the interdiffusion, the superconducting transition temperature
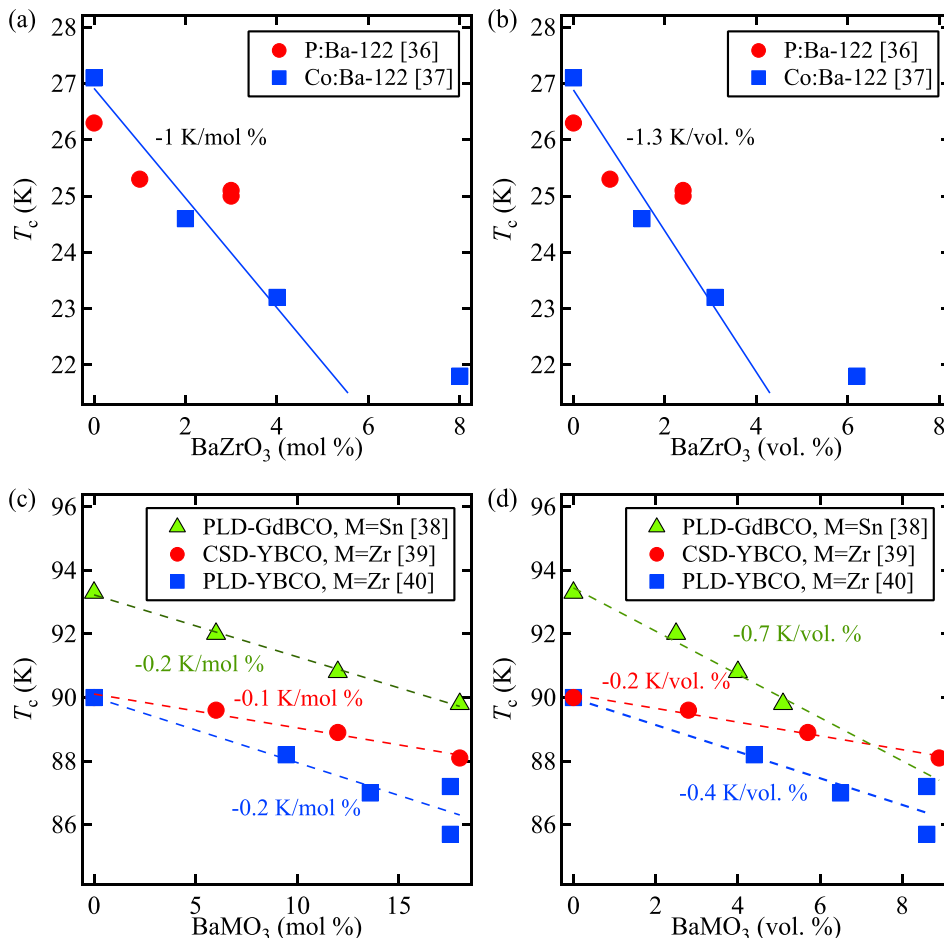

FIG. 6. (a) Superconducting transition temperature of P-doped Ba-122 (P:Ba-122)[36] and Co-doped Ba-122 (Co:Ba-122)[37] as a function of BaZrO₃ content. For P:Ba-122, the zero resistance temperature $T_{c,0}$ is plotted, whereas the onset $T_{c,onset}$ is plotted for Co:Ba-122. (b) The same plot as a function of BaZrO₃ volume fraction. (c) Reduction of the T_c for GdBa₂Cu₃O₇ (GdBCO) grown by PLD[38] and YBa₂Cu₃O₇ (YBCO) grown by chemical solution deposition (CSD)[39] and PLD[40] as a function of BaMO₃ (M: Zr and Sn). (d) The same plot as a function of BaMO₃ volume fraction. Compared to the PLD-processed YBCO, the CSD-processed YBCO showed a gentle reduction of T_c around −0.1 K/mol. % (−0.2 K/vol. %).
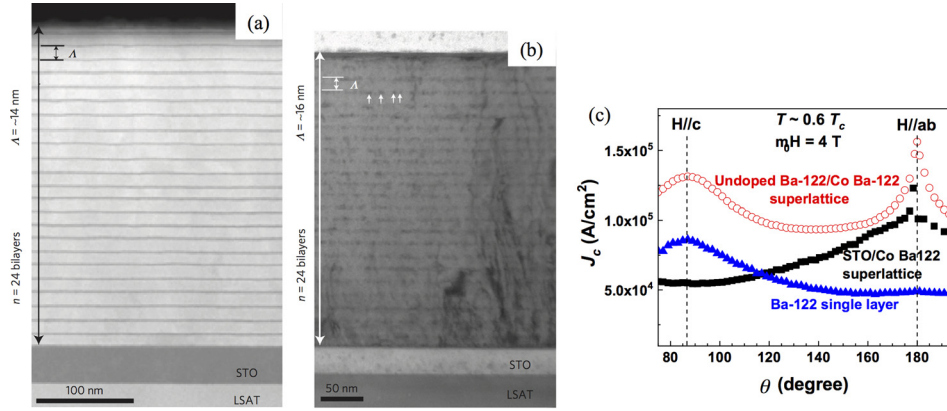
FIG. 7. Cross sectional TEM image of (a) the SrTiO$_3$/Co-doped Ba-122 superlattice and (b) the undoped oxygen-rich Ba-122/Co-doped Ba-122 superlattice. Reproduced with permission from Lee *et al.*, Nat. Mater. **12**, 392–396 (2013). Copyright 2013 Spring Nature. (c) Angular dependence of J_c of the SrTiO$_3$/Co-doped Ba-122 and the undoped Ba-122/Co-doped Ba-122 superlattices measured at a reduced temperature of $T = 0.6T_c$ and 4 T. For comparison, the data of the single layer of Co-doped Ba-122 were also plotted. The figure is redrawn with some modifications based on the data taken from Fig. 5(c) in Ref. 42.

of the FeSe/FeTe superlattice was improved compared to FeSe (i.e., from 12 K for FeSe on CaF$_2$ to 15.8 K for FeSe/FeTe superlattice on CaF$_2$). No information on critical current densities was reported on these films.

Besides introducing artificial pinning centers, the multi-layer approach can improve the superconducting properties.[44–46] Tarantini *et al.* reported Co-doped, BaO-added Ba-122/Co-doped Ba-122 multilayer fabricated on CaF$_2$(001) substrate for which the superconducting transition temperature was increased by compressive strain.[44] Pinning force densities as high as 84 and 70 G N/m^3 for $H \parallel ab$ and $\parallel c$ at 4.2 K were achieved by a combination of short c-axis nanorods, round nanoparticles, and ab-arranged precipitates.

Engelmann *et al.* fabricated Co:Ba-122 (20 nm)/Fe (4 nm)/Co:Ba-122 (20 nm)/Fe (30 nm) multilayers on MgAl$_2$O$_4$, which showed a high T_c of 29.4 K due probably to an As-deficiency.[45] Chen *et al.* reported the enhancement of in-field performance for an Fe(Se,Te) double layer with a CeO$_2$ insertion layer on SrTiO$_3$.[46] The improvement is ascribed to the additional interfacial defects introduced by the insertion layer.

3. Irradiation

Although many irradiation experiments on FBS single crystals have been reported, only few studies except for 11 report on the effects of irradiation in thin films (see Table II). An excellent review article on radiation effects in FBS has recently been published by Eisterer.[57] Here, we will briefly summarize the available data on FBS thin films.

The defects created by fast neutron irradiation on Fe(Se,Te) thin films produced only a small impact on the superconducting properties (T_c, upper critical field, H_{c2}, irreversibility field, H_{irr} and J_c).[47] On the other hand, low-energy proton irradiation created nanoscale compressive strain, resulting in an increase in T_c by 0.5 K.[48] Additionally, cascade defects combined with nanoscale strain worked as strong vortex pinning centers, and consequently J_c increased by one order of magnitude at 12 K and by a factor of 2 at 4.2 K at fields around and above 15 T. Ozaki *et al.* also investigated the effect of Au irradiation on the superconducting

properties of Fe(Se,Te) thin films.[49] The Au-irradiated film showed a slight decrease in T_c by 0.5 K. However, in-field J_c properties were improved for all field orientations at 4.2 K. Furthermore, the J_c enhancement was nearly 70% compared to the pristine film at 10 K and 9 T. Ahmad *et al.* reported the effect of proton irradiation on the superconducting properties of FeSe$_{1-x}$Te$_x$ ($x = 0.4$, 0.55) thin films.[50] The reduction of superconducting properties was caused by the local heating, which may accelerate the displacement of atoms and create vacancies. Sylva *et al.* pointed out the importance of the position where the proton is implanted: the improvement of J_c up to 50% at 12 K and 7 T was observed when protons were accumulated far from the film/substrate interface. Simultaneously, T_c and H_{c2} were unaltered.[51] On the other hand, superconducting properties were degraded when the proton-implanted layer was close to the interface.

Non-superconducting FeTe thin films were irradiated by oxygen ions.[52] At the maximum dose of 1×10^{17} cm^{-2}, the FeTe film was amorphous.

The effect of 3 MeV proton irradiation on the superconducting properties of Co-doped Ba-122 was reported by Maiorov *et al.*[53] After the irradiation (total dose of 2×10^{16} cm^{-2}), the T_c decreased by only 1 K. Overall, J_c for the irradiated film was decreased in low field. At high field and low temperatures, J_c was increased, particularly for J_c

TABLE II. Radiation experiments on FBS thin films reported so far.

Material	Particles	Total or max. dose (cm^{-2})	Change in T_c (K)	Ref.
Fe(Se,Te)	Fast neutrons	1.2×10^{17}	−0.3	47
Fe(Se,Te)	190 KeV protons	1.2×10^{17}	+0.5	48
Fe(Se,Te)	6 MeV Au	1.0×10^{12}	−0.5	49
Fe(Se,Te)	3.5 MeV protons	5.0×10^{15}	−7.0	50
Fe(Se,Te)	3.5 MeV protons	7.3×10^{16}	−0.6	51
FeTe	150 KV O	1.0×10^{17}	N.A.	52
Co-doped Ba-122	3 MeV protons	2.0×10^{16}	−1.0	53
Co-doped Ba-122	200 KeV protons	1.8×10^{15}	−18	54
P-doped Ba-122	250 MeV Au	7.3×10^{11}	−0.8	55
NdFeAs(O,F)	2 MeV He	5.0×10^{15}	−3.0	56

($H \parallel ab$) due to a clear anisotropic contribution from the point-like defects.

The effect of proton irradiation on Co-doped Ba-122 thin films was also reported by Schilling *et al.*, who investigated the disorder-induced symmetry change from $s\pm$ to s_{++} by THz spectroscopy.[54] On the assumption that the electron-electron coupling constant is positive, disorder induces a transition between $s\pm$ and s_{++} states.[58] In this report, they observed such a transition: the small gap was closed at a certain amount of disorder and re-opened again by further increase in disorder. These results suggested that the superconducting order parameter in the pristine film has $s\pm$ symmetry. However, no information on H_{c2}, H_{irr}, and J_c was reported.

Daghero *et al.* reported on the effect of irradiation with 250-MeV Au ions on the superconducting properties of optimally P-doped Ba-122 thin films fabricated by MBE.[55] The residual resistivity at $T = 0\,K$ (ρ_0) increased with dose level, whilst the decrease in T_c was only $0.8\,K$ for a maximum dose of $7.26 \times 10^{11}\,cm^{-2}$. Such a small reduction in T_c would indicate $s\pm$ symmetry. The authors also considered the role of the substrate in the radiation effect: Au ion irradiation and heating in the substrate may have caused additional damage.

Unlike in NdFeAs(O,F) single crystals,[59] α-particle irradiation on NdFeAs(O,F) thin films did not create Kondo-like defects,[56] suggesting that the type of defects induced by this type of irradiation is also strongly affected by other factors, the most likely being the initial composition. In the irradiated NdFeAs(O,F) films, an increase in both H_{c2} and H_{irr} were observed. However, only for $H \parallel c$, a moderate improvement in J_c was found, whereas for $H \parallel ab$ point-defects compete with intrinsic pinning, reducing J_c.

III. GRAIN BOUNDARIES

There are two main purposes for experiments on FBS thin films fabricated on bicrystal substrates having a single well-defined grain boundary. One is to realize Josephson junctions with two FBS electrodes for fundamental research and assessing their potential for electronics applications. The other goal is to check the J_c transparency across the grain boundary, which is vital information for wire applications. In the former experiments, thin films are prepared on bicrystal substrates with relatively large misorientation angle θ_{GB} to realize an SNS (superconductor–normal–superconductor) or SIS (superconductor–insulator–superconductor) junction. It is worth mentioning that all bicrystal experiments on FBS reported to date have been conducted using symmetric [001]-tilt bicrystal substrates (SrTiO$_3$, MgO, and LSAT). Hence, grain boundary experiments using different types of bicrystals (i.e., valley- or roof-type [010]-tilt and [100]-twist) are necessary to obtain deeper knowledge of grain boundary characteristics of FBS, since inter-grain J_c (J_c^{GB}) depends, in general, on the GB type, as shown for YBa$_2$Cu$_3$O$_7$ deposited on various types of bicrystals.[60] In general, different results are expected in case of different order parameter symmetry (e.g., s-wave or d-wave) as well as strain sensitivity and charge density.

To date, for FBS there have been only a few systematic and extended bicrystal experiments on Fe(Se,Te) and Co-doped Ba-122 films. Only singular experiments on P-doped Ba-122 (Ref. 34) and recently on NdFeAs(O,F)[61] have been reported so far, Table III. Reviews on GB properties in FBS bulk and film samples in comparison to high-T_c cuprate superconductors have been given by Deutscher in 2010 (Ref. 62) and Durrell *et al.* in 2011.[63] In Subsections III A and III B, we review all reported bicrystal experiments on FBS concerning Josephson junctions followed by inter-grain J_c reduction due to weak-link behaviour. Some of the experiments mentioned below have been conducted for both purposes of Josephson junctions and investigation of the J_c transparency across the grain boundary. Therefore, occasionally the same experiments are referred to in Secs. III A and III B.

A. Josephson junctions with two FBS electrodes

1. Fe(Se,Te)

To date, four bicrystal experiments on Fe(Se,Te) have been published. First, bicrystal experiments on Fe(Se,Te) were reported by Sarnelli *et al.*, who fabricated 150 nm thick Fe(Se,Te) films on [001]-tilt SrTiO$_3$ bicrystals with a misorientation angle (θ_{GB}) of 45° by PLD using a Nd:YAG laser with a wave length of 1024 nm.[64] The authors made microbridges (2.6–20 μm wide and 20 μm long) on Fe(Se,Te) bicrystals by optical lithography and ion beam milling. To avoid possible damage during the process, the sample holder was cooled to −40 °C. The I–V characteristics at 4.2 K showed a resistively shunted junction (RSJ) behavior with a low normal-state resistance R_N in the range of $40\,m\Omega \leq R_N \leq 270\,m\Omega$, which is typical for SNS junctions. Compared to the cuprates, those values are two orders of magnitude lower. As a result, the $I_c R_N$ product was 18–33 μV, where I_c is the Josephson critical current. Later, Sarnelli *et al.* fabricated dc superconducting quantum interference devices (dc-SQUIDs) using 100-nm thick Fe(Se,Te) bicrystal with $\theta_{GB} = 24°$.[65,66] The resultant device showed a clear voltage modulation under magnetic field with a maximum amplitude of 3.8 μV at 4.2 K.

TABLE III. Summary of bicrystal experiments on Fe-based superconductors. All of these experiments have been conducted using [001]-tilt bicrystal substrates.

Materials	Deposition	Substrates	θ_{GB} (deg)	θ_c (deg)
Fe(Se,Te)	PLD	SrTiO$_3$ (Refs. 64–67)	4–45	9 (Refs. 65 and 67)
Co-doped Ba-122	PLD	SrTiO$_3$ (Refs. 68 and 69)	3–30	<6 (Ref. 68)
Co-doped Ba-122	PLD	MgO,[70–72] LSAT[70,71,73,74]	3–45	9 (Refs. 70 and 71)
P-doped Ba-122	MBE	MgO,[34] LSAT[75]	24, 45	N.A.
NdFeAs(O,F)	MBE	MgO[61]	6–45	<6

Si *et al.* fabricated 100 nm thick Fe(Se,Te) thin films on CeO_2-buffered $SrTiO_3$ bicrystal substrates ($\theta_{GB} = 4°$, 7°, 15°, and 24°) by PLD.[67] Microbridges with 300 μm length and 20–25 μm width were fabricated by laser cutting for transport measurements. The ρ–T curve of the bridge with $\theta_{GB} = 24°$ showed a double superconducting transition at 20 K and 17.5 K with $\rho = 0$ at around 12 K. On the other hand, the bridge with $\theta_{GB} = 4°$ had one transition at 20 K similar to the intra-grain bridge. Using the bridge with $\theta_{GB} = 24°$, the authors observed multiple Josephson current modulations by magnetic field. The magnitude of the I_c modulation was around 80%. The I–V characteristics at 2 K roughly followed the RSJ model with a normal state resistance of $R_N = 28$ mΩ. Such a low value of R_N is due to the metallic nature of the normal state of the Fe(Se,Te) bicrystal grain boundary junction. The $I_c R_N$ product of their junctions was estimated to around 22 μV at 2 K.

2. Co- and P-doped Ba-122

Katase *et al.* reported on Josephson junctions and dc-SQUIDs in PLD-processed Co-doped Ba-122 ($T_c = 21.5$–22.6 K) using LSAT bicrystal substrates with $\theta_{GB} = 30°$.[73,74] For single Josephson junctions, the authors fabricated micro-bridges (10 μm wide and 300 μm long) by photolithography and Ar ion milling. The I–V characteristics of the resultant junction at 4.2 K showed RSJ behavior. The normal state resistance R_N of the junction was around 12 mΩ, resulting in a low $I_c R_N$ product of ~50 μV. For dc-SQUIDs, bridges with a smaller width of 3 μm (area of SQUID loop was 18×8 μm^2) were made to reduce the critical current. The resultant device showed a clear voltage modulation with an amplitude of 1.4 μV at 14 K. However, the shape of V-Φ deviated from the ideal sinusoidal function. Additionally, the level of flux noise at 1 Hz was ~4.3×10^{-4} Φ_0Hz$^{-1/2}$, which was one order of magnitude higher than for cuprates. From those junction experiments, the barrier layer is of metallic nature in Co-doped Ba-122. Indeed, the inter-grain J_c^{GB} showed a quadratic temperature dependence, indicative of SNS rather than SIS junctions.[70] Hence, for realizing practical SQUIDs, it is necessary to increase the junction resistance R_N by an artificial insulating barrier.

Schmidt *et al.* also reported on PLD-grown Co-doped Ba-122 grain boundary junctions using $SrTiO_3$ with $\theta_{GB} = 30°$.[69] To suppress oxygen diffusion from $SrTiO_3$, a 10 nm thick $MgAl_2O_4$ layer was deposited on the $SrTiO_3$ bicrystal. Fe-buffer layer followed by Co-doped Ba-122 were deposited on this template. All layers were epitaxially grown as confirmed by XRD. In their junctions ($T_c = 24$ K), a high excess current ($I_{ex} = 645$ μA) was observed, and therefore a small $I_c R_N$ product of 6.5 μV at 4.2 K was obtained.

Sakagami *et al.* prepared P-doped Ba-122 by MBE on [001]-tilt MgO bicrystals with $\theta_{GB} = 24°$.[34] The I–V characteristics of their device ($T_c = 29.5$ K, bridge width of 30 μm) at 2 K was described by a flux-flow extension of the RSJ model, which gave a normal state resistance of $R_N = 4.4$ mΩ and a Josephson critical current of $I_c = 8.5$ mA. As a consequence, a small $I_c R_N$ product of 37 μV was obtained. Such a low normal state resistance of the junction is again due to the metallic nature of the grain boundary. The same group also fabricated P-doped Ba-122 thin films on LSAT bicrystals with $\theta_{GB} = 45°$.[75] The I–V characteristics of the resultant junction can again be fitted by a RSJ model with flux flow current. Their device had an $I_c R_N$ product of 45 μV at 4.2 K. However, this value was corrected to 11 μV by taking into account the excess current.

3. Summary of Josephson junctions with two FBS electrodes

All bicrystal junctions of Fe(Se,Te), Co-doped, and P-doped Ba-122 have the same low level of $I_c R_N$ (tens of μV) compared to that of YBCO (on the order of mV at 4.2 K). The main reason for such low $I_c R_N$ is that the barrier layer is of metallic nature, which leads to a low junction resistance R_N. Therefore, the dc-SQUIDs made from Fe(Se,Te)[65] and Co-doped Ba-122 (Ref. 74) showed high flux noise. The properties mentioned above are not suitable for electronics applications, however, are highly beneficial to wire applications. To realize electronics applications like SQUIDs, one would have to increase the R_N by an artificial insulating barrier. Interested readers for Josephson effects in FBS may refer to Ref. 76.

B. Misorientation dependence of inter-grain J_c

1. Fe(Se,Te)

The inter-grain J_c of Fe(Se,Te) across a $\theta_{GB} = 45°$ grain boundary without magnetic field was around ~10^4 A/cm^2 at 4.2 K, one order of magnitude lower than the intra-grain J_c (J_c^{GB}).[64] These results suggested that the decay of J_c with GB angle may not be as strong as for the cuprates, where at this angle the suppression is significant (4 orders of magnitude). Later, Sarnelli *et al.* have reported J_c^{GB}/J_c^{Grain} as a function of θ_{GB}.[65] It was found that the θ_{GB} dependence of J_c^{GB}/J_c^{Grain} is almost similar to the result reported by Si *et al.*[67] Additionally, the level of J_c^{GB} was almost constant for $\theta_{GB} = 24°$ and $\theta_{GB} = 45°$, which will be discussed later.

Si *et al.* found that J_c^{GB} for $\theta_{GB} = 4°$ and 7° maintained ~10^5 A/cm^2 even in the presence of large applied magnetic fields ($\mu_0 H = 10$ T, $H \parallel c$) at 4.2 K, indicative of strong links in this θ_{GB} range.[67] On the other hand, J_c^{GB} for $\theta_{GB} > 15°$ was significantly suppressed by a small magnetic field: J_c^{GB} for $\theta_{GB} = 24°$, e.g., was reduced from 4×10^4 to 7×10^3 A/cm^2 even by a small magnetic field of $\mu_0 H = 0.5$ mT. Based on the experimental results above, the authors concluded that the critical angle θ_c was around 9°.

2. Co- and P-doped Ba-122

Already in the early stage of thin film research of pnictide superconductors, Lee *et al.* reported on the weak-link behavior of [001] tilt GBs in Co-doped Ba-122.[68] They fabricated 350-nm thick films (T_c over 20 K) on $SrTiO_3$ bicrystals ($\theta_{GB} = 3°$, 6°, 9°, and 24°) by PLD. Low-temperature laser scanning microscopy (LTLSM) and magneto-optical imaging (MOI) on these Co-doped Ba-122 bicrystal junctions with $\theta_{GB} = 6°$ and 9° revealed the weak-link behavior also for low-angle GBs (Fig. 8). As can be seen in Fig. 8(a), a
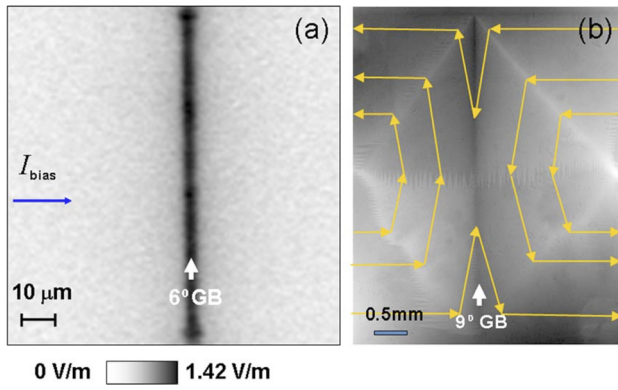
FIG. 8. (a) LTLSM image scanned in 1 μm steps of a 6° [001]-tilt bicrystal taken at 12 K and 0.25 T with bias current of 39 mA which generated 17 V across the bridge. (b) MO image of a 9° bicrystal with computed streamlines yellow of the magnetization current calculated from the Bean model. The MO image was taken after cooling to 6 K in a perpendicular field of 120 mT and then reducing the field to zero. Reproduced with the permission from Appl. Phys. Lett. 95, 212505 (2009). Copyright 2009 AIP Publishing LLC.

large dissipation across the 6° grain boundary was detected by LTLSM. For the 9° grain boundary sample, two clear roof-top shapes separated by the grain boundary are observed by MOI [Fig. 8(b)]. These results indicated that the critical angle θ_c may be below 6°, which differs from the results reported two years later by Katase et al.[70] We speculate that oxygen impurities may have limited the J_c^{GB} for these Co-doped Ba-122 films on SrTiO₃. In fact, it is likely that the nanorods (see Sec. II A 1) tend to segregate along the GB reducing the effective cross-section and consequently J_c. Detailed microstructural investigations are necessary to identify such differences.

Later Katase, Hiramatsu et al. reported a θ_c as large as 9° from their detailed bicrystal experiments on Co-doped Ba-122.[70,71] Here, the respective T_c of Co-doped Ba-122 were 20.7 K on MgO and 21.6 K on LSAT bicrystals. Shown in Fig. 9 is the θ_{GB} dependence of inter-grain J_c measured at

4 K without magnetic field. Clearly, the inter-grain J_c remained at 1 MA/cm² up to $\theta_{GB} = 9°$. Beyond this angle, the decay of inter-grain J_c sets in. Another interesting feature is that J_c^{GB} was almost constant for $\theta_{GB} = 30°$ and $\theta_{GB} = 45°$.

A high inter-grain J_c over 1 MA/cm² even at $\theta_{GB} = 24°$ and 4 K was reported by Sakagami et al.[34] for a P-doped Ba-122 thin film grown by molecular beam epitaxy (MBE) on a MgO bicrystal substrate. Although the number of data points is not sufficient, P-doped Ba-122 most likely also has a higher critical angle than the cuprates.

It was reported that polycrystalline K-doped Ba-122 bulk samples showed a large self-field J_c of ∼0.1 MA/cm².[78] Microstructural analysis revealed that the grain boundaries were clean without segregation of impurities. Later, atom probe tomography performed on both K- and Co-doped Ba-122 polycrystals revealed that traces of oxygen impurities were present at the GBs, in particular, for the Co-doped sample (Fig. 10).[77] Such oxidized regions may hide the intrinsic characteristics of the grain boundary. Although the microstructures of Co-doped and K-doped Ba-122 polycrystalline samples are almost identical, the in-field J_c performance of Co-doped Ba-122 is inferior to that of K-doped Ba-122 at 4.2 K.[78] These results indicate that grain boundary properties depend on the kind of doping elements (i.e., K, Co, and P) and perhaps AE in AEBa₂As₂ too. Therefore, grain boundary experiments on K-doped Ba- and Sr-122 are highly desirable and also important for on-going development of powder-in-tube (PIT) processed wires and bulk magnets.[79]

3. NdFeAs(O,F)

LnFeAs(O,F) (Ln = Sm and Nd) compounds have the highest T_c among the FBS. Hence, a lot of effort was devoted for producing LnFeAs(O,F) wires. However, the self-field J_c of polycrystalline SmFeAs(O,F) was only ∼4 × 10⁴ A/cm² at 4.2 K,[80] which is one order of magnitude lower than for K-doped Ba-122, indicative of possible weak-link behavior. Hence, bicrystal experiments on LnFeAs(O,F) have been long desired to elucidate this question.
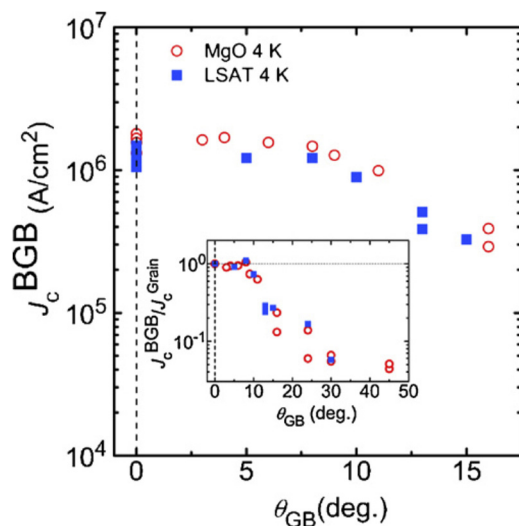

FIG. 9. The θ_{GB} dependence of inter-grain J_c for Co-doped Ba-122 bicrystals measured at 4 K without magnetic field. Reproduced with permission from Hiramatsu et al., Mater. Sci. Eng., B 177, 515–519 (2012). Copyright 2012 Elsevier.
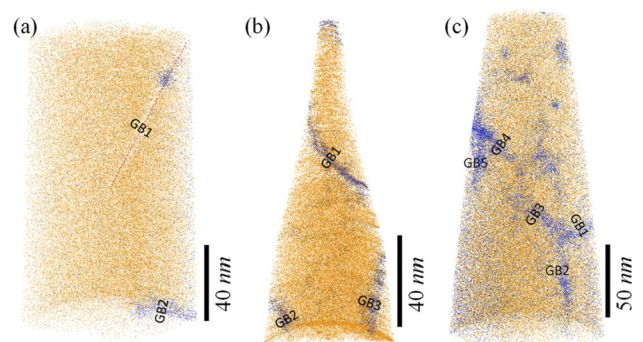
FIG. 10. A 3-D atom-probe tomographic reconstruction of: (a) (Ba₀.₆K₀.₄)Fe₂As₂; (b) Ba₀.₄K₀.₆; and (c) Ba(Fe₀.₉₂Co₀.₀₈)₂As₂ superconductors. Oxygen atoms are in blue and Ba atoms are in orange, other elements are excluded for a clear display of grain boundary segregation. Each dot represents a single atom, but not to scale. Reproduced with permission from Appl. Phys. Lett. 105, 162604 (2014). Copyright 2014 AIP Publishing LLC.

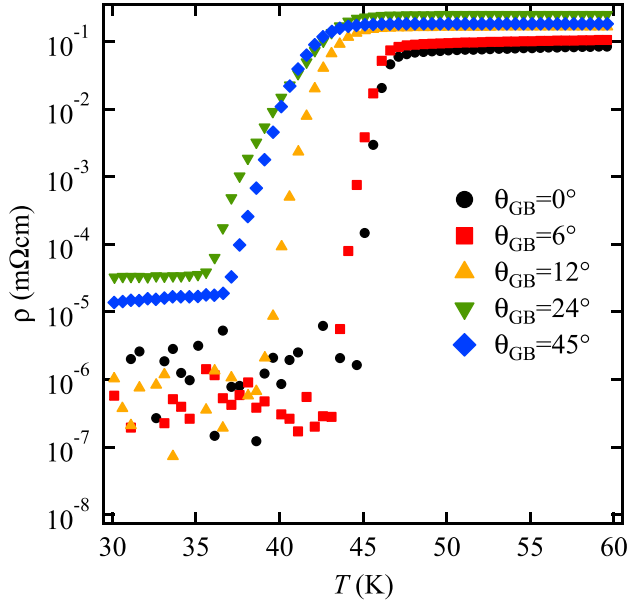FIG. 11. Semi-logarithmic plot of the resistivity curves for NdFeAs(O,F) bicrystals having different θ_{GB}. $\theta_{GB} = 0°$ represents the intra-grain J_c. The figure is redrawn with some modifications based on the data taken from Fig. 3(b) in Ref. 61.

Omura *et al*. have recently reported on the GB angle dependence of transport properties for NdFeAs(O,F) thin films fabricated by MBE.[61] For $\theta_{GB} = 6°$ and $12°$, the resistivity in the superconducting state was below the instrumental limitation (Fig. 11). For $\theta_{GB} \geq 24°$, in contrast a finite resistivity below T_c was observed and hence the inter-grain J_c was zero. The inter-grain J_c for $\theta_{GB} = 6°$ was reduced by nearly 30% compared to the intra-grain J_c. Hence, the critical angle for these NdFeAs(O,F) films was less than $6°$. However, the authors stated that the results did not reflect the intrinsic grain boundary properties due to the erosion of the grain boundaries by fluorine diffusion.

4. Summary of the misorientation dependence of inter-grain J_c

Shown in Fig. 12 is a summary of the θ_{GB} dependence of inter-grain J_c for various FBS bicrystals. Clearly, P-doped Ba-122 showed a high inter-grain J_c of 1 MA/cm^2 at θ_{GB} = 24° [Fig. 12(a)], which is highly beneficial for wire applications. It is also noted that J_c^{GB} for Ba-122 is higher than for YBCO beyond $\theta_{GB} = 24°$. Although intra-grain and inter-grain J_c are high for P-doped Ba-122, the θ_{GB} dependence of

J_c^{GB} is similar to that of Co-doped Ba-122 [Fig. 12(b)]. For all FBS except for NdFeAs(O,F), the critical angle θ_c is around $9°$, which indicates that in-plane misorientation alignments of FBS grains less than $9°$ usually do not impede the critical current flow. Hence, one can expect that grain boundary networks whose in-plane misorientation is less than $9°$ work as flux pinning centers. Indeed, the pinning force density analysis of P-doped Ba-122 on technical substrates revealed that the GB pinning contribution is dominant for $H \parallel c$,[83,84] which will be discussed later.

The initial slope for the J_c decrease with angle for FBS is almost similar to that of YBCO, Fig. 12(b), which is different from the common belief. A distinct difference between FBS and YBCO is recognized above $\theta_{GB} = 24°$: for YBCO, J_c^{GB} continuously decreases exponentially with θ_{GB}, whilst J_c^{GB} remains constant for FBS. This may be due to the different symmetry: *d*-wave for YBCO and sign reversal *s*-wave for FBS. Additionally, the grain boundaries for both Ba-122 and Fe(Se,Te) are of metallic nature. Another plausible reason may be 45° [001]-tilt GBs in Ba-122 and Fe(Se,Te) compounds being special, low-Σ or facetted GBs with a narrower structurally and electronically disturbed region than for GBs with smaller θ_{GB} as discussed for high-T_c cuprates.[85]

It is reported that inter-grain J_c for YBCO is ameliorated by Ca-doping for which the depletion of the carrier density at GBs is compensated.[86] Later, electron energy loss spectroscopy (EELS) revealed high concentrations of Ca at the tensile regions of the GBs.[87] On the assumption that the same mechanism could work for overdoped Ba-122, Durrell *et al*. fabricated Co-doped Ba-122 bicrystals with Co concentration from 8% (optimal) to 10% (overdoped).[63] However, no improvement of inter-grain J_c was observed. More of such experiments should be conducted to tackle the GB problem for FBS.

IV. FBS THIN FILMS ON TECHNICAL SUBSTRATES

As described in Sec. III B, grain boundaries are less critical an issue for FBS than for cuprates, and powder-in-tube-processed wires based on 11, 122, and 1111 have been fabricated. Among them, the in-field J_c of 122 wires has already reached the practical level of 10^5 A/cm^2,[99] and a 120 m long tape of K-doped Sr-122 has been realized.[100] However, biaxially textured films on single-crystalline substrates and also single crystals[21] showed superior J_c–H performance to polycrystalline samples. To date, seven groups have published
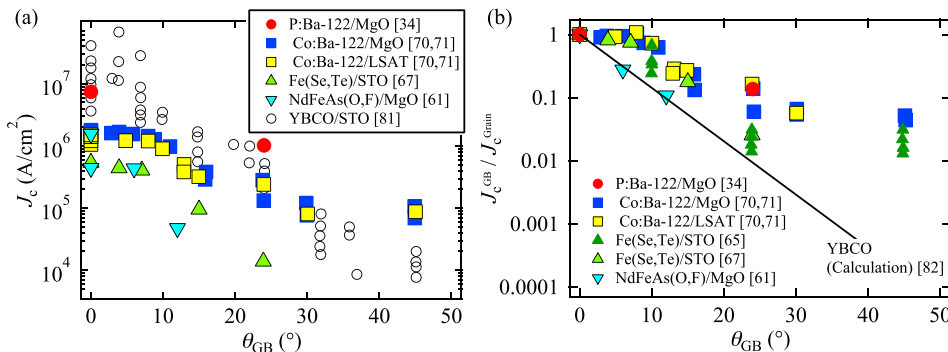
FIG. 12. The θ_{GB} dependence of inter-grain J_c for various FBS bicrystals. The data were acquired at 4 K for P:Ba-122 (Ref. 34) and Co:Ba-122,[70,71] whereas for Fe(Se,Te)[65,67] and NdFeAs(O,F)[61] the measurements were conducted at 4.2 K. For comparison, the data of YBa$_2$Cu$_3$O$_7$ (YBCO) measured at 4 K were also plotted.[81] (b) The ratio of J_c^{GB}/J_c^{Grain} as a function of θ_{GB} for various FBS. The black line represents YBCO and was taken from Ref. 82.

TABLE IV. FBS thin films on technical substrates reported by BNL (Brookhaven National Laboratory), IEE-CAS (Institute of Electrical Engineering, Chinese Academy of Sciences), CNR (Consiglio Nazionale delle Ricerche Genova) NIMS (National Institute of Materials Science), IFW (Leibniz Institute for Solid State and Materials Research Dresden), TIT (Tokyo Institute of Technology), and Nagoya (Nagoya University). LMO and EC depo. stand for LaMnO$_3$ and Electrochemical deposition, respectively.

Group	Materials	Substrates	Methods	T_c (K)	J_c performance
BNL	Fe(Se,Te)[88]	IBAD-MgO	PLD	$T_{c,R=0} = 11$	$>1 \times 10^4$ A/cm^2 at 25 T, 4.2 K
	Fe(Se,Te)[89]	RABiTS with CeO$_2$	PLD	$T_c^{onset} = 20$	0.1 MA/cm^2 at 30 T, 4.2 K
IEE-CAS	Fe(Se,Te)[90]	IBAD-MgO with LMO	PLD	16.8	0.43 MA/cm^2 at self-field, 4.2 K
CNR	Fe(Se,Te)[91]	RABiTS with CeO$_2$	PLD	18	$>2 \times 10^4$ A/cm^2 at 18 T, 4.2 K
NIMS	FeSe[92]	RABiTS	EC depo.	8	N/A
	FeSe[93]	RABiTS	EC depo.	$T_c^{onset} = 8.4$ $T_{c,R=0} = 2.5$	N/A
IFW	Co:Ba-122 (Ref. 94)	IBAD-MgO	PLD	$T_c^{onset} = 21$	0.1 MA/cm^2 at self-field, 8 K
	Co:Ba-122 (Ref. 95)	IBAD-MgO	PLD	$T_{c,50\%} = 23$	0.1 MA/cm^2 at 9 T, 4.2 K
TIT	Co:Ba-122 (Ref. 96)	IBAD-MgO	PLD	$T_c^{onset} = 22.0$	0.1 MA/cm^2 at 9 T, 4.2 K
IEE-CAS	Co:Ba-122 (Ref. 97)	IBAD-MgO with LMO	PLD	$T_{c,onset} = 20.2$	0.86 MA/cm^2 at 9 T, 4.2 K
TIT	P:Ba-122 (Ref. 83)	IBAD-MgO	PLD	$T_c^{onset} = 26$	$>0.11 \times 10^4$ A/cm^2 at 9 T, 4.2 K
	P:Ba-122 (Ref. 83)	IBAD-MgO	PLD	$T_c^{onset} = 23$	0.2×10^4 A/cm^2 at 9 T, 4.2 K
TIT	P:Ba-122 (Ref. 7)	IBAD-MgO 15 cm long	PLD	$T_{c,10\%} = 18.0$	$I_c = 0.47$ mA at self-field
	P:Ba-122 (Ref. 7)	IBAD-MgO short tape	PLD	$T_{c,10\%} = 24.0$	$I_c = 975$ mA at self-field
TIT	P:Ba-122 (Ref. 84)	IBAD-MgO	PLD	$T_{c,90\%} = 28$	0.1 MA/cm^2 at 15 T, 4.2 K
Nagoya	NdFeAs(O,F)[98]	IBAD-MgO	MBE	43	7×10^4 cm^{-2} at self-field, 5 K

results on FBS films on technical substrates as prototype coated conductor samples, as summarized in Table IV. In this section, various FBS thin films on technical substrates are reviewed. Most of these studies were done on IBAD-MgO templates (textured MgO templates are prepared on Hastelloy by ion beam assisted deposition), supplied by iBeam, Inc., USA and Shanghai Creative Supercond. Technol. Co. Ltd., China. Three studies on FeSe and Fe(Se,Te) used RABiTS (rolling-assisted biaxially textured substrate) template for which two of them were supplied by ENEA (Italian National Agency for New Technologies, Energy and Sustainable Economic Development) and evico GmbH, Germany. The other has been fabricated by in-house R&D collaboration between Brookhaven National Laboratory and Oak Ridge National Laboratory.

A. FeSe and Fe(Se,Te)

Despite the large lattice mismatch between Fe(Se,Te) ($a_{Fe(Se,Te)} = 3.81$ Å) and MgO ($a_{MgO} = 4.21$ Å), epitaxial Fe(Se,Te) thin films were successfully fabricated on hastelloy tapes, on which epitaxial MgO templates were deposited by IBAD.[88] The respective in-plane and out-of-plane full width at half maximum of Fe(Se,Te) were $\Delta\phi = 4.5°$ and $\Delta\omega = 3.5°$. Clearly, $\Delta\phi = 4.5°$ is less than the critical angle θ_c for [001]-tilt Fe(Se,Te) grain boundaries. Although a critical angle for [010]-tilt Fe(Se,Te) grain boundary junctions has not been reported, it is expected that [001]-tilt and [010]-tilt GBs in Fe(Se,Te) have a similar critical angle due to the small anisotropy and likely the sign reversal s-wave type symmetry. Therefore, weak-link behavior is absent in these Fe(Se,Te) films on IBAD-MgO. The lower T_c ($T_{c,R=0} = 11$ K) of that film compared to the film on LaAlO$_3$ substrate ($\sim$15 K) is mostly ascribed to the large lattice misfit. The Fe(Se,Te) film showed an almost isotropic J_c over 10^4 A/cm^2 at 25 T and 4.2 K. The pinning force analysis revealed that point defect pinning governs the J_c–H properties.

To further improve J_c-H properties of Fe(Se,Te) on technical substrate, Si et al. have fabricated Fe(Se,Te) thin films on CeO$_2$-buffered RABiTS.[89] The lattice parameter of CeO$_2$ is around 3.82 Å ($\sim$5.41/$\sqrt{2}$), which almost perfectly matches the in-plane lattice parameter of Fe(Se,Te). As a result, Fe(Se,Te) on RABiTS showed a high onset T_c of over 20 K with a sharp transition of 1 K width. The structural characterization by X-ray diffraction revealed an in-plane FWHM $\Delta\phi_{Fe(Se,Te)} = 6°$. Despite the larger in-plane texture spread, the Fe(Se,Te) film was capable of carrying large current densities (Fig. 13). A nearly isotropic $J_c \sim 0.1$ MA/cm^2 at 4.2 K and 30 T was observed. The pinning mechanism was the same as for the Fe(Se,Te) film on IBAD-MgO. The authors concluded that the use of CeO$_2$ buffer layer is the key for achieving high T_c. Additionally, the substrates containing low angle grain boundaries up to 7° do not impede the critical current flow, which is different from REBa$_2$Cu$_3$O$_7$.

Quite recently, the group of IEE-CAS reported Fe(Se,Te) thin films on IBAD-MgO with LaMnO$_3$ (LMO)
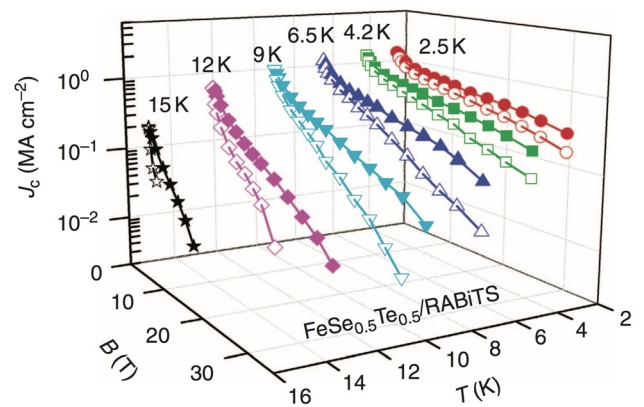

FIG. 13. The field dependence of J_c for an Fe(Se,Te) film deposited on RABiTS measured at various temperatures. Closed and open symbols represent $H \parallel c$ and $\parallel ab$, respectively. Reproduced with permission from Si et al., Nat. Commun. **4**, 1347 (2013). Copyright 2013 Spring Nature.

buffer layers.[90] The Fe(Se,Te) was grown on LMO with cube-on-cube configuration. The respective out-of-plane and in-plane full width at half maximum values of Fe(Se,Te) are $\Delta\omega = 3.4°$ and $\Delta\phi = 7.8°$. The T_c of the sample is 16.8 K, which is slightly higher than that of bulk due to the compressive strain. Albeit the large $\Delta\phi$ of 7.8°, an in-field J_c above 0.35 MA/cm^2 up to 9 T was recorded at 4.2 K. Additionally, the anisotropy of J_c was relatively small.

The group of CNR (Consiglio Nazionale delle Ricerche) has been recently working on an attempt to decrease the number of necessary buffer layers or exchanging the metallic substrate to less expensive materials. Both solutions may reduce the fabrication costs of such Fe(Se,Te) coated conductors.[91] The films on Ni5W RABiTS covered with a single CeO$_2$ buffer layer (produced by ENEA) showed a T_c of ~18 K and isotropic J_c above 2×10^4 A/cm^2 at 4.2 K in fields up to 18 T. On biaxially textured invar (nickel-iron alloy with 36 mass% of Ni) tape, epitaxial Fe(Se,Te) layers of the same texture quality as the tape itself (FWHM ~ 9°) were grown without any buffer layer. The superconducting properties of these samples still have to be investigated.

The group at NIMS proposed a unique technique for fabricating FeSe films on RABiTS provided by evico GmbH.[92,93] They performed electrochemical deposition using three electrodes, Pt (counter electrode), Ag/AgCl (reference electrode), and RABiTS (working electrode) at 70 °C. The electrolyte was prepared from a solution of FeCl$_2$ · 4H$_2$O, SeO$_2$, and Na$_2$SO$_4$ in distilled water. A pH value of 2.1 for the electrode was maintained during the deposition. X-ray diffraction confirmed FeSe phase formation without heat treatment. Although the resulting film had a low T_c of 2.5 K, this technique is promising for further development and optimization.[93]

B. Co- and P-doped Ba-122

The first report on Co-doped Ba-122 on technical substrates was published by Iida et al.[94] They fabricated Co-doped Ba-122 films on Fe-buffered IBAD-MgO templates by PLD. Due to the relatively large in-plane mosaicity of the MgO ($\Delta\phi_{MgO} \sim 6°$), the crystalline quality of the intermediate Fe as well as Co-doped Ba-122 layers was poor (i.e., $\Delta\phi_{Fe} \sim 5°$ and $\Delta\phi_{Ba-122} \sim 5°$). Although biaxially textured Co-doped Ba-122 showed an onset T_c of 21 K, the in-field J_c at 8 K was almost one order of magnitude lower compared to the film on single crystalline MgO due to the poor crystalline quality. Later, employing a high-quality MgO template ($\Delta\phi_{MgO} \sim 2.4°$) improved the in-field J_c of Co-doped Ba-122 to a level almost comparable to films on single crystalline substrates.[95]

Almost at the same time, Katase et al. also reported on the fabrication of Co-doped Ba-122 directly on IBAD-MgO.[96] A sharp texture of the Co-doped Ba-122 with $\Delta\phi_{Ba122} \sim 3.2°-3.5°$ was obtained irrespective of the in-plane mosaicity of MgO templates due to the self-epitaxy effect. The onset T_c of Co-doped Ba-122 on IBAD-MgO was 22 K. In-field J_c reached almost 0.1 MA/cm^2 under 9 T at 4 K.

Very recently, Co-doped Ba-122 was also fabricated on IBAD-MgO with LMO by Xu et al.[97] They used SrTiO$_3$ as buffer layer between LMO and Co-doped Ba-122. The

resultant film showed almost isotropic J_c. The respective J_c for $H \parallel c$ and $\parallel ab$ were 0.86 and 0.96 MA/cm^2 at 9 T and 4.2 K.

P-doped Ba-122 shows the second highest T_c among the 122 compounds and, therefore, J_c-H properties are usually superior to Co-doped Ba-122. Additionally, growth-related and artificial pinning centers can be introduced into the P-doped Ba-122 matrix as discussed in Sec. II B 1. Sato et al. fabricated P-doped Ba-122 thin films with PLD on IBAD-MgO with two different in-plain texture qualities, $\Delta\phi_{MgO} = 4°$ and $8°$.[83] The structural characterization by X-ray diffraction revealed $\Delta\phi_{Ba-122} = 2.7°$ and $8°$ for P-doped Ba-122 deposited on the well and poorly textured MgO template, respectively. The film on poor crystalline MgO template had an onset T_c of 23 K, which is comparable to the Co-doped Ba-122 on IBAD-MgO [Fig. 14(a)]. On the other hand, the P-doped Ba-122 on the well textured MgO template had a higher T_c of 26 K [Fig. 14(a)]. The low-T_c sample showed nonetheless better in-field J_c properties: almost isotropic J_c exceeding 0.1 MA/cm^2 at 9 T and 4 K [Fig. 14(b)]. This can be explained by grain boundary pinning. Figure 15 shows the J_c–H properties of a further optimized P-doped Ba-122 thin film on IBAD-MgO ($T_{c,90\%Rn}$ of 28.3 K) and the corresponding normalized pinning force density (f_p) as a function of $h = H/H_{max}$, where H_{max} is the field at which the pinning force density (F_p) shows the maximum value.[84] As can be seen, f_p curves for $H \parallel c$ at different temperatures almost fall onto a master curve described by

$$f_p = \frac{25}{16} h^{0.5} \left(1 - \frac{h}{5}\right)^2. \tag{2}$$

This formula is analogous to

$$\left(\frac{H}{H_{irr}}\right)^p \left(1 - \frac{H}{H_{irr}}\right)^q \tag{3}$$

($p = 0.5$, $q = 2$, and H_{irr} is the irreversibility field) found by Dew-Hughes for pinning by 2D defects such as grain boundaries.[101] Recently, Paturi et al. found that the exponent $p = 0.5$ for YBCO regardless of q for a defect size on the order of the coherence length.[102] On the other hand, p increases to 1 with increasing defect size. This confirms that
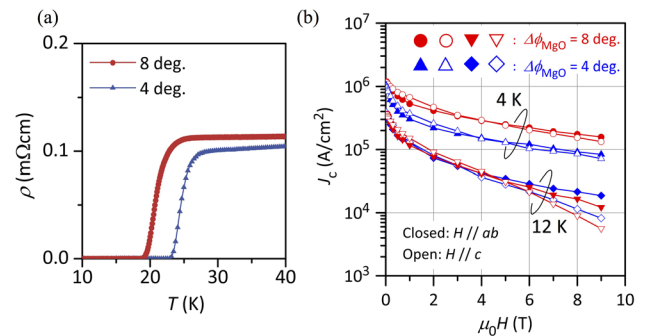

FIG. 14. (a) The temperature dependence of resistivity for P-doped Ba-122 deposited on IBAD-MgO with different in-plain mosaicities, $\Delta\phi_{MgO} = 4°$ and $8°$. (b) The corresponding in-field J_c-H properties of these films measured at 4 K and 12 K. Reproduced with permission from Sato et al., Sci. Rep. **6**, 36828 (2016). Copyright 2016 Spring Nature.
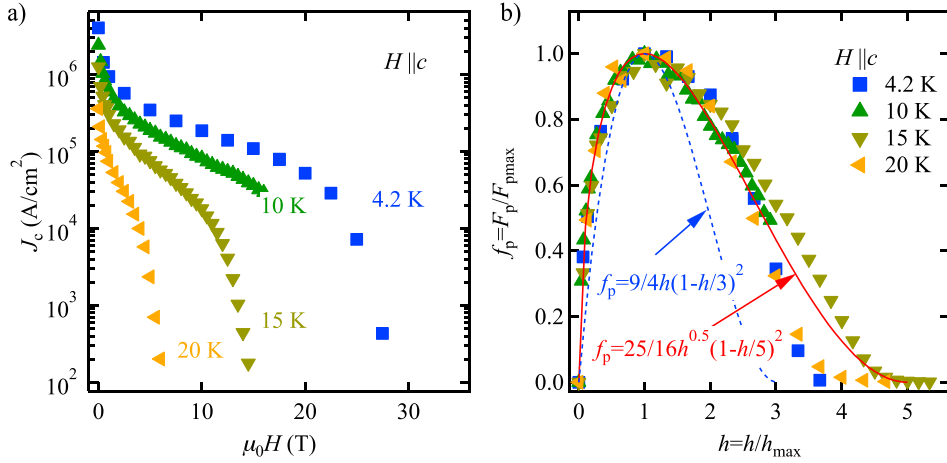
FIG. 15. (a) J_c-H properties of a P-doped Ba-122 on IBAD-MgO measured at different temperatures for $H \parallel c$. (b) The corresponding normalized pinning force density (f_p) as a function of reduced field h. The solid line is for 2D defects such as grain boundaries, and the dotted line is for 3D defects such as point-like defects. The figure is redrawn with some modifications based on the data taken from Fig. 5 in Ref. 84.

the pinning in P-doped Ba-122 on IBAD-MgO is dominated by the dislocations with nano-size.

Hosono's group even fabricated a 10 cm long P-doped Ba-122 tape using a reel-to-reel system by PLD,[7] although the growth conditions were not fully optimized. The resultant film showed a slightly lower $T_{c,10\%Rn}$ of 18.7 K and a low I_c of 0.47 mA per cm-width at 4.2 K, corresponding to a J_c of 4.7×10^4 A/cm^2. They also found that even short samples had a low T_c. To improve the superconducting properties, they fabricated Fe$_3$P/P-doped Ba-122 bilayers on IBAD-MgO. As a result, the superconducting properties were improved to $T_{c,10\%Rn} = 24$ K and $I_c = 975$ mA per cm-width ($J_c = 1.75 \times 10^5$ A cm^2) at 4.2 K.

C. NdFeAs(O,F)

Biaxially textured NdFeAs(O,F) films on IBAD-MgO have been fabricated by MBE at Nagoya University.[98] The 102 peak ϕ-scan revealed a small amount of 45° rotated grains. Shown in Fig. 16 are J_c–H properties of NdFeAs(O,F) for $H \parallel c$ in comparison to data on PIT-processed SmFeAs(O,F) wires and a NdFeAs(O,F) film on

single crystal MgO. Here, J_c of NdFeAs(O,F) on IBAD-MgO was calculated from the hysteresis loops using the Bean model. The NdFeAs(O,F) thin film on IBAD template had a self-field J_c of 7×10^4 A/cm^2 at 5 K, whereas the corresponding value for PIT-processed SmFeAs(O,F) was around 4×10^4 A/cm^2 at 4.2 K.[103] Now, the performance gap between the tape and wire is very small. However, given that J_c of NdFeAs(O,F) on single crystalline MgO substrates is above 10^4 A/cm^2 at 4.2 K even at fields as high as at 35 T and self-field values reach 3 MA/cm^2,[25] there is certainly room for further improvement of superconducting properties of NdFeAs(O,F) on IBAD-MgO. The reason for the low J_c values on IBAD templates is most likely the strong F diffusion in the GB regions, as revealed by bicrystal experiments, see Sec. III B 3.

D. Summary of FBS thin films on technical substrates

Figure 17 compares J_c–H characteristics at 4.2 K of various FBS thin films on technical substrates and of high-quality FBS thin films on single-crystalline substrates. For Co-doped Ba-122, although low-field J_c for the film on IBAD[97] is lower than that for the film on single crystal,[44] a crossover is visible at 7.5 T. As can be seen in Fig. 17(b), in-field J_c performance for the P-doped Ba-122 on IBAD-MgO[84] is slightly inferior to the film on MgO single-crystalline substrate[22] [Fig. 17(b)]. Such a difference in J_c–H for the P-doped Ba-122 is mainly explained by the fact that the films on single-crystalline substrates are pinning-improved. It is expected that similar microstructures transferred to tapes would lead to similar J_c levels. Additionally, the phase formation has to be optimized so that the full potential of the films on single crystals can be achieved on tape. On the other hand, J_c–H of Fe(Se,Te) on RABiTS[89] is almost comparable to that of the pinning-enhanced Fe(Se,Te) thin film[48] [Fig. 17(c)]. Finally, the largest discrepancy is seen for NdFeAs(O,F) on IBAD-MgO and single crystalline MgO [Fig. 17(d)], which can be explained by the strong F diffusion along GBs and a concomitant broadening of their regions. This might be improved by employing fluorine-free oxygen-deficient LnFeAsO compounds.

To evaluate the best possible J_c performance, the ultimate critical current density, i.e., depairing current density at
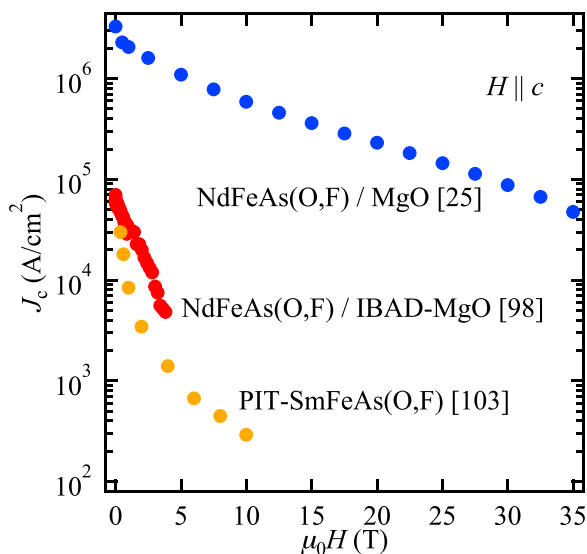

FIG. 16. The J_c-H properties of the NdFeAs(O,F) on IBAD-MgO at 5 K (Ref. 98) in comparison to the data of PIT-processed SmFeAs(O,F) wires[103] and a NdFeAs(O,F) thin film on single crystal MgO[25] at 4.2 K.
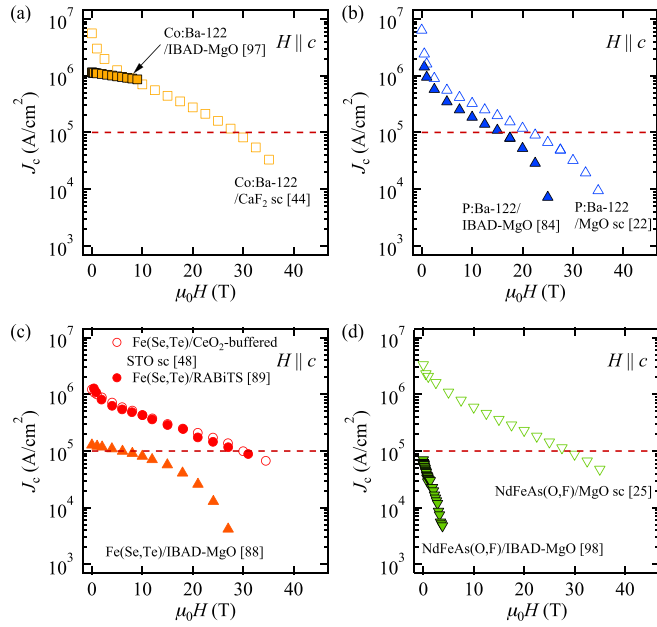
FIG. 17. J_c-H properties of various FBS thin films on technical substrates and single crystalline substrates. Measurement temperature was 4.2 K except for NdFeAs(O,F) on IBAD-MgO. The applied magnetic field was $H \parallel c$: (a) Co:Ba-122 on IBAD-MgO[97] and pinning enhanced Co:Ba-122 on CaF$_2$ fabricated by PLD.[44] (b) P:Ba-122 on IBAD-MgO[84] by PLD and MBE-processed P:Ba-122.[22] (c) Fe(Se,Te) on IBAD-MgO[88] and RABiTS.[89] Pinning enhanced Fe(Se,Te) on CeO$_2$-buffered SrTiO$_3$.[48] All films were fabricated by PLD. (d) NdFeAs(O,F) on IBAD-MgO[98] at 5 K and MgO single crystalline substrate fabricated by MBE.[25]

4.2 K [J_d (4.2 K)] for various FBS estimated by Eqs. (4) and (5) is tabulated in Table V

$$J_d(0) = \frac{\phi_0}{3\sqrt{3}\pi\mu_0\lambda_{ab}^2(0)\xi_{ab}(0)}, \quad (4)$$

$$J_d(T) = J_d(0)\left\{1 - \left(\frac{T}{T_c}\right)^2\right\}^{1.5}\left\{1 + \left(\frac{T}{T_c}\right)^2\right\}. \quad (5)$$

Clearly, Ba-122 compounds possess the highest J_d (4.2 K) among the FBS. The maximum achievable J_c by core pinning is around 30% of the depairing current density.[104] However, the pinning efficiency, here defined as $J_c^{s.f.}/J_d$, at 4.2 K for FBS even on single crystalline substrates reaches only 3.5%–5.8%.

V. SUMMARY AND DISCUSSION

In order to understand the performance potential of FBS, we discussed the main application-related properties

TABLE V. Physical quantities of Fe(Se,Te), Co- and P-doped Ba-122, and NdFeAs(O,F) used for the calculations of the $J_c^{s.f.}/J_d$ at 4.2 K for FBS films on single crystals.

Materials	λ_{ab} (0) (nm)	ξ_{ab} (0) (nm)	J_d (4.2 K) (MA/cm^2)	$J_c^{s.f.}/J_d$ (%) at 4.2 K
Fe(Se,Te)	430 (Ref. 11)	1.5 (Ref. 11)	34	3.5
Co-doped Ba-122	190 (Ref. 105)	2.76 (Ref. 105)	100	5.6
P-doped Ba-122	200 (Ref. 13)	2.14 (Ref. 13)	117	5.4
NdFeAs(O,F)	270 (Ref. 14)	2.4 (Ref. 14)	57	5.8

like pinning improvement by natural and artificial defects, the transparency of grain boundaries, and the properties of GB networks. Naturally grown defects [BaFeO$_2$ in Co-doped Ba-122 and threading dislocations in Fe(Se,Te)] mainly contribute to the c-axis correlated pinning, and point pinning introduced by strain is beneficial as well. Artificial pinning centers can be introduced in the superconducting matrix by multilayer deposition, irradiation, and the addition of nano-particles such as BaZrO$_3$ to the PLD targets. Although all methods described here are effective for improving in-field properties, the J_c level at 4.2 K achieved so far is still only up to ~6% of the depairing current density in films on single crystals, suggesting room for further improvement of superconducting properties of FBS.

Bicrystal experiments on Ba-122 and Fe(Se,Te) revealed the metallic nature of grain boundaries. The critical angle above which inter-grain J_c falls off is around 9°. However, the initial slope for the logarithmic J_c decrease with GB angle for FBS is similar to that of YBCO. A distinct difference between FBS and YBCO is recognised above θ_{GB} = 24°: for YBCO J_c^{GB} continuously decreases with θ_{GB}, whilst J_c^{GB} remains constant for FBS. Overall, those properties are highly beneficial for making cheap FBS conductors.

The three main systems with largest application potential (11, 122, and 1111) have already been realized on technical substrates. Most of the FBS coated conductor prototypes showed a comparable T_c to their counterparts on single-crystalline substrates. Fe(Se,Te) and P-doped Ba-122 reached the practical level (0.1 MA/cm^2 at 15 T). It is noted that PIT-processed FBS wires (K-doped Ba-122 and Sr-122) also have reached this level,[8] despite the presence of many GBs. Therefore, further GB experiments on FBS, especially for K-doped 122, are desired. To further improve the in-field J_c properties of FBS on technical substrates, the introduction of artificial pinning centers without compromising T_c is necessary.

Even though FBS tapes will never compete with YBCO tapes regarding their superconducting properties, they could compete with YBCO in terms of cost. For YBCO tapes, expensive highly textured metallic substrates and Ag layers to allow oxygenation are necessary. However, FBS can be realized on poorly textured templates without expensive cover layers. For realizing FBS conductors, there are other properties that need to be evaluated: (i) thick FBS thin films (~1 μm) on technical substrates should be fabricated and characterized for realizing FBS coated conductors. (ii) Strain tolerance dependence of J_c should be investigated, which is important for making a magnet.

[1] Y. Kamihara, T. Watanabe, M. Hirano, and H. Hosono, "Iron-based layered superconductor La[O$_{1-x}$F$_x$]FeAs ($x = 0.05 - 0.12$) with $T_c = 26$ K," J. Am. Chem. Soc. 130, 3296–3297 (2008).

[2] Q. Li, W. Si, and I. K. Dimitrov, "Films of iron chalcogenide superconductors," Rep. Prog. Phys. 74, 124510 (2011).

[3] H. Hiramatsu, T. Katase, T. Kamiya, and H. Hosono, "Thin film growth and device fabrication of iron-based superconductors," J. Phys. Soc. Jpn. 81, 011011 (2012).

[4] P. Mele, "Superconducting properties of iron chalcogenide thin films," Sci. Technol. Adv. Mater. 13, 054301 (2012).

[5] S. Haindl, M. Kidszun, S. Oswald, C. Hess, B. Büchner, S. Kölling, L. Wilde, T. Thersleff, V. V. Yurchenko, M. Jourdan, H. Hiramatsu, and H. Hosono, "Thin film growth of Fe-based superconductors: From fundamental properties to functional devices. A comparative review," Rep. Prog. Phys. 77, 046502 (2014).

[6] Y. Imai, F. Nabeshima, and A. Maeda, "Comparative review on thin film growth of iron-based superconductors," Condens. Matter 2, 25 (2017).

[7] H. Hosono, K. Tanabe, E. Takayama-Muromachi, H. Kageyama, S. Yamanaka, H. Kumakura, M. Nohara, H. Hiramatsu, and S. Fujitsu, "Exploration of new superconductors and functional materials, and fabrication of superconducting tapes and wires of iron pnictides," Sci. Technol. Adv. Mater. 16, 033503 (2015).

[8] H. Hosono, A. Yamamoto, H. Hiramatsu, and Y. Ma, "Recent advances in iron-based superconductors towards applications," Mater. Today 21, 278–302 (2018).

[9] M. Sakoda, K. Iida, and M. Naito, "Recent progress in thin-film growth of Fe-based superconductors: Superior superconductivity achieved by thin films," Supercond. Sci. Technol. 31, 093001 (2018).

[10] H. Yang, G. Chen, X. Zhu, J. Xing, and H.-H. Wen, "BCS-like critical fluctuations with limited overlap of Cooper pairs in FeSe," Phys. Rev. B 96, 064501 (2017).

[11] T. Klein, D. Braithwaite, A. Demuer, A. Knafo, G. Lapertot, C. Marcenat, P. Rodière, I. Sheikin, P. Strobel, P. Sulpice, and P. Toulemonde, "Thermodynamic phase diagram of Fe(Se$_{0.5}$Te$_{0.5}$) single crystals in fields up to 28 Tesla," Phys. Rev. B 82, 184506 (2010).

[12] A. Yamamoto, J. Jaroszynski, C. Tarantini, L. Balicas, J. Jiang, A. Gurevich, D. C. Larbalestier, R. Jin, A. S. Sefat, M. A. McGuire, B. C. Sales, D. K. Christen, and D. Mandrus, "Small anisotropy, weak thermal fluctuations, and high field superconductivity in Co-doped iron pnictide Ba(Fe$_{1-x}$Co$_x$)$_2$As$_2$," Appl. Phys. Lett. 94, 062511 (2009).

[13] C. Chaparro, L. Fang, H. Claus, A. Rydh, G. W. Crabtree, V. Stanev, W. K. Kwok, and U. Welp, "Doping dependence of the specific heat of single-crystal BaFe$_2$(As$_{1-x}$P$_x$)$_2$," Phys. Rev. B 85, 184525 (2012).

[14] J. Kacmarcik, C. Marcenat, T. Klein, Z. Pribulova, C. J. van der Beek, M. Konczykowski, S. K. Bud'ko, M. Tillman, N. Ni, and P. C. Canfield, "Strongly dissimilar vortex-liquid regimes in single-crystalline NdFeAs(O,F) and (Ba,K)Fe$_2$As$_2$: A comparative study," Phys. Rev. B 80, 014515 (2009).

[15] J. Jaroszynski, S. C. Riggs, F. Hunte, D. C. L. A. Gurevich, G. S. Boebinger, F. F. Balakirev, A. Migliori, Z. A. Ren, W. Lu, J. Yang, X. L. Shen, X. L. Dong, Z. X. Zhao, R. Jin, A. S. Sefat, M. A. McGuire, B. C. Sales, D. K. Christen, and D. Mandrus, "Comparative high-field magneto-transport of the oxypnictide superconductors RFeAsO$_{1-x}$F$_x$ (R = La, Nd) and SmFeAsO$_{1-\delta}$," Phys. Rev. B 78, 064511 (2008).

[16] M. Zehetmayer, M. Eisterer, J. Jun, S. M. Kazakov, J. Karpinski, A. Wisniewski, and H. W. Weber, "Mixed-state properties of superconducting MgB$_2$ single crystal," Phys. Rev. B 66, 052505 (2002).

[17] M. Putti, I. Pallecchi, E. Bellingeri, M. R. Cimberle, M. Tropeano, C. Ferdeghini, A. Palenzona, C. Tarantini, A. Yamamoto, J. Jiang, J. Jaroszynski, F. Kametani, D. Abraimov, A. Polyanskii, J. D. Weiss, E. E. Hellstrom, A. Gurevich, D. C. Larbalestier, R. Jin, B. C. Sales, A. S. Sefat, M. A. McGuire, D. Mandrus, P. Cheng, Y. Jia, H. H. Wen, S. Lee, and C. B. Eom, "New Fe-based superconductors: Properties relevant for applications," Supercond. Sci. Technol. 23, 034003 (2010).

[18] G. Blatter, M. V. Feigel'man, V. B. Geshkenbein, A. I. Larkin, and V. M. Vinokur, "Vortices in high-temperature superconductors," Rev. Mod. Phys. 66, 1125–1388 (1994).

[19] S. Eley, M. Miura, B. Maiorov, and L. Civale, "Universal lower limit on vortex creep in superconductors," Nat. Mater. 16, 409–413 (2017).

[20] S. Lee, J. Jiang, Y. Zhang, C. W. Bark, J. D. Weiss, C. Tarantini, C. T. Nelson, H. W. Jang, C. M. Folkman, S. H. Baek, A. Polyanskii, D. Abraimov, A. Yamamoto, J. W. Park, X. Q. Pan, E. E. Hellstrom, D. C. Larbalestier, and C. B. Eom, "Template engineering of Co-doped BaFe$_2$As$_2$ single-crystal thin films," Nat. Mater. 9, 397–402 (2010).

[21] S. Ishida, D. Song, H. Ogino, A. Iyo, H. Eisaki, M. Nakajima, J. Shimoyama, and M. Eisterer, "Doping-dependent critical current properties in K, Co, and P-doped BaFe$_2$As$_2$ single crystals," Phys. Rev. B 95, 014517 (2017).

[22] F. Kurth, C. Tarantini, V. Grinenko, J. Hänisch, J. Jaroszynski, E. Reich, Y. Mori, A. Sakagami, T. Kawaguchi, J. Engelmann, L. Schultz, B. Holzapfel, H. Ikuta, R. Hühne, and K. Iida, "Unusually high critical current of clean P-doped BaFe$_2$As$_2$ single crystalline thin film," Appl. Phys. Lett. 106, 072602 (2015).

[23] K. Iida, J. Hänisch, M. Schulze, S. Aswartham, S. Wurmehl, B. Büchner, L. Schultz, and B. Holzapfel, "Generic Fe buffer layers for Fe-based superconductors: Epitaxial FeSe$_{1-x}$Te$_x$ thin films," Appl. Phys. Lett. 99, 202503 (2011).

[24] Y. Sun, T. Taen, Y. Tsuchiya, Q. Ding, S. Pyon, Z. Shi, and T. Tamegai, "Large, homogeneous, and isotropic critical current density in oxygen-annealed Fe$_{1+y}$Te$_{0.6}$Se$_{0.4}$ single crystal," Appl. Phys. Express 6, 043101 (2013).

[25] C. Tarantini, K. Iida, J. Hänisch, F. Kurth, J. Jaroszynski, N. Sumiya, M. Chihara, T. Hatano, H. Ikuta, S. Schmidt, P. Seidel, B. Holzapfel, and D. C. Larbalestier, "Intrinsic and extrinsic pinning in NdFeAs(O,F): Vortex trapping and lock-in by the layered structure," Sci. Rep. 6, 36047 (2014).

[26] M. Eisterer, V. Mishev, M. Zehetmayer, N. D. Zhigadlo, S. Katrych, and J. Karpinski, "Critical current anisotropy in Nd-1111 single crystals and the influence of neutron irradiation," Supercond. Sci. Technol. 27, 044009 (2014).

[27] K. Matsumoto and P. Mele, "Artificial pinning center technology to enhance vortex pinning in YBCO coated conductors," Supercond. Sci. Technol. 23, 014001 (2010).

[28] C. Tarantini, S. Lee, Y. Zhang, J. Jiang, C. W. Bark, J. D. Weiss, A. Polyanskii, C. T. Nelson, H. W. Jang, C. M. Folkman, S. H. Baek, X. Q. Pan, A. Gurevich, E. E. Hellstrom, C. B. Eom, and D. C. Larbalestier, "Strong vortex pinning in Co-doped BaFe$_2$As$_2$ single crystal thin films," Appl. Phys. Lett. 96, 142510 (2010).

[29] C. Tarantini, S. Lee, F. Kametani, J. Jiang, J. D. Weiss, J. Jaroszynski, C. M. Folkman, E. E. Hellstrom, C. B. Eom, and D. C. Larbalestier, "Artificial and self-assembled vortex-pinning centers in superconducting Ba(Fe$_{1-x}$Co$_x$)$_2$As$_2$ thin films as a route to obtaining very high critical-current densities," Phys. Rev. B 86, 214504 (2012).

[30] Y. Zhang, C. T. Nelson, S. Lee, J. Jiang, C. W. Bark, J. D. Weiss, C. Tarantini, C. M. Folkman, S. H. Baek, E. E. Hellstrom, D. C. Larbalestier, C. B. Eom, and P. X, "Self-assembled oxide nanopillars in epitaxial BaFe$_2$As$_2$ thin films for vortex pinning," Appl. Phys. Lett. 98, 042509 (2011).

[31] E. Bellingeri, S. Kawale, I. Pallecchi, A. Gerbi, R. Buzio, V. Braccini, A. Palenzona, M. Putti, M. Adamo, E. Sarnelli, and C. Ferdeghini, "Strong vortex pinning in FeSe$_{0.5}$Te$_{0.5}$ epitaxial thin film," Appl. Phys. Lett. 100, 082601 (2012).

[32] H. Sato, H. Hiramatsu, T. Kamiya, and H. Hosono, "High critical-current density with less anisotropy in BaFe$_2$(As,P)$_2$ epitaxial thin films: Effect of intentionally grown c-axis vortex-pinning centers," Appl. Phys. Lett. 104, 182603 (2014).

[33] J. Hänisch, K. Iida, F. Kurth, T. Thersleff, S. Trommler, E. Reich, R. Hühne, L. Schultz, and B. Holzapfel, "The effect of 45° grain boundaries and associated Fe particles on J_c and resistivity in Ba(Fe$_{0.9}$Co$_{0.1}$)$_2$As$_2$ thin films," AIP Conf. Proc. 1574, 260 (2014).

[34] A. Sakagami, T. Kawaguchi, M. Tabuchi, T. Ujihara, Y. Takeda, and H. Ikuta, "Critical current density and grain boundary property of BaFe$_2$(As,P)$_2$ thin films," Phys. C 494, 181–184 (2013).

[35] J. L. MacManus-Driscoll, S. R. Foltyn, Q. X. Jia, H. Wang, A. Serquis, L. Civale, B. Maiorov, M. E. Hawley, M. P. Maley, and D. E. Peterson, "Strongly enhanced current densities in superconducting coated conductors of YBa$_2$Cu$_3$O$_{7-x}$ + BaZrO$_3$," Nat. Mater. 3, 439–443 (2004).

[36] M. Miura, B. Maiorov, T. Kato, T. Shimode, K. Wada, S. Adachi, and K. Tanabe, "Strongly enhanced flux pinning in one-step deposition of BaFe$_2$(As$_{0.66}$P$_{0.33}$)$_2$ superconductor films with uniformly dispersed BaZrO$_3$ nanoparticles," Nat. Commun. 4, 2499 (2013).

[37] J. Lee, J. Jiang, F. Kametani, M. J. Oh, J. D. Weiss, Y. Collantes, S. Seo, S. Yoon, C. Tarantini, Y. J. Jo, E. E. Hellstrom, and S. Lee, "High critical current density over 1 MA cm^{-2} at 13 T in BaZrO$_3$ incorporated Ba(Fe,Co)$_2$As$_2$ thin film," Supercond. Sci. Technol. 30, 085006 (2017).

[38] V. Chepikov, N. Mineev, P. Degtyarenko, S. Lee, V. Petrykin, A. Ovcharov, A. Vasiliev, A. Kaul, V. Amelichev, A. Kamenev, A. Molodyk, and S. Samoilenkov, "Introduction of BaSnO$_3$ and BaZrO$_3$ artificial pinning centres into 2G HTS wires based on PLD-GdBCO films.

Phase I of the industrial R&D programme at SuperOx," Supercond. Sci. Technol. **30**, 124001 (2017).

[39] I. Birlik, M. Erbe, T. Freudenberg, E. Celik, L. Schultz, and B. Holzapfel, "Flux pinning improvement of YBCO superconducting films with BaZrO$_3$ nanoparticles prepared by chemical solution deposition method," J. Phys.: Conf. Ser. **234**, 012004 (2010).

[40] T. Horide, F. Kametani, S. Yoshioka, T. Kitamura, and K. Matsumoto, "Structural evolution induced by interfacial lattice mismatch in self-organized YBa$_2$Cu$_3$O$_{7-\delta}$ nanocomposite film," ACS Nano **11**, 1780–1788 (2017).

[41] A. Goyal, S. Kang, K. J. Leonard, P. M. Martin, A. A. Gapud, M. Varela, M. Paranthaman, A. O. Ijaduola, E. D. Specht, J. R. Thompson, D. K. Christen, S. J. Pennycook, and F. A. List, "Irradiation-free, columnar defects comprised of self-assembled nanodots and nanorods resulting in strongly enhanced flux-pinning in YBa$_2$Cu$_3$O$_{7-\delta}$ films," Supercond. Sci. Technol. **18**, 1533 (2005).

[42] S. Lee, C. Tarantini, P. Gao, J. Jiang, J. D. Weiss, F. Kametani, C. M. Folkman, Y. Zhang, X. Q. Pan, E. E. Hellstrom, D. C. Larbalestier, and C. B. Eom, "Artificially engineered superlattices of pnictide superconductors," Nat. Mater. **12**, 392–396 (2013).

[43] F. Nabeshima, Y. Imai, A. Ichinose, I. Tsukada, and A. Maeda, "Growth and transport properties of FeSe/FeTe superlattice thin films," Jpn. J. Appl. Phys., Part 1 **56**, 020308 (2017).

[44] C. Tarantini, F. Kametani, S. Lee, J. Jiang, J. D. Weiss, J. Jaroszynski, E. E. Hellstrom, C. B. Eom, and D. C. Larbalestier, "Development of very high J_c in Ba(Fe$_{1-x}$Co$_x$)$_2$As$_2$ thin films grown on CaF$_2$," Sci. Rep. **4**, 7305 (2014).

[45] J. Engelmann, K. Iida, F. Kurth, C. Behler, S. Oswald, R. Hühne, B. Holzapfel, L. Schultz, and D. Haindl, "Fe/Ba(Fe$_{1-x}$Co$_x$)$_2$As$_2$ multilayers and quasi-multilayers with $T_c = 29$ K," Phys. C **494**, 185–188 (2013).

[46] L. Chen, C. F. Tsai, Y. Zhu, A. Chen, Z. Bi, J. Lee, and H. Wang, "Enhanced flux pinning properties in superconducting FeSe$_{0.5}$Te$_{0.5}$ thin films with secondary phases," Supercond. Sci. Technol. **25**, 025020 (2012).

[47] M. Eisterer, R. Raunicher, H. W. Weber, E. Bellingeri, M. R. Cimberle, I. Pallecchi, M. Putti, and C. Ferdeghini, "Anisotropic critical currents in FeSe$_{0.5}$Te$_{0.5}$ films and the influence of neutron irradiation," Supercond. Sci. Technol. **24**, 065016 (2011).

[48] T. Ozaki, L. Wu, C. Zhang, J. Jaroszynski, W. Si, J. Zhou, Y. Zhu, and Q. Li, "A route for a strong increase of critical current in nanostrained iron-based superconductors," Nat. Commun. **7**, 13036 (2016).

[49] T. Ozaki, L. Wu, C. Zhang, W. Si, Q. Jie, and Q. Li, "Enhanced critical current in superconducting FeSe$_{0.5}$Te$_{0.5}$ films at all magnetic field orientations by scalable gold ion irradiation," Supercond. Sci. Technol. **31**, 024002 (2018).

[50] D. Ahmad, W. J. Choi, Y. I. Seo, S. Seo, S. Lee, T. Park, J. Mosqueira, G. Gu, and Y. S. Kwon, "Effect or proton irradiation on the fluctuation-induced magnetoconductivity of FeSe$_{1-x}$Te$_x$ thin films," New J. Phys. **19**, 093004 (2017).

[51] G. Sylva, E. Bellingeri, C. Ferdeghini, A. Martinelli, I. Pallecchi, L. Pellegrino, M. Putti, G. Ghigo, L. Gozzelino, D. Torsello, G. Grimaldi, A. Leo, A. Nigro, and V. Braccini, "Effects of high energy proton irradiation on the superconducting properties of Fe(Se,Te) thin films," Supercond. Sci. Technol. **31**, 054001 (2018).

[52] J. Janaki, T. Kumar, A. Mani, E. P. Amaladass, N. Raveendran, P. Magudapathy, S. Kalavathi, T. N. Sairam, and T. R. Ravindran, "Characterization and low temperature study of iron telluride thin films upon ageing and oxygen ion irradiation," J. Supercond. Novel Magn. **27**, 2639–2643 (2014).

[53] B. Maiorov, T. Katase, O. Usov, M. Weigand, L. Civale, H. Hiramatsu, and H. Hosono, "Competition and cooperation of pinning by extrinsic point-like defects and intrinsic strong columnar defects in BaFe$_2$As$_2$ thin films," Phys. Rev. B **86**, 094513 (2012).

[54] M. B. Schilling, A. Baumgartner, B. Gorshunov, E. S. Zhukova, V. A. Dravin, K. V. Misten, D. V. Efremov, O. V. Dolgov, K. Iida, M. Dressel, and S. Zapf, "Tracing the s$\pm$ symmetry in iron pnictides by controlled disorder," Phys. Rev. B **93**, 174515 (2016).

[55] D. Daghero, M. Tortello, L. Gozzelino, R. S. Gonnelli, T. Hatano, T. Kawaguchi, and H. Ikuta, "Effect of ion irradiation on surface morphology and superconductivity of BaFe$_2$(As$_{1-x}$P$_x$)$_2$ films," Appl. Surf. Sci. **395**, 9–15 (2017).

[56] C. Tarantini, K. Iida, N. Sumiya, C. Chihara, T. Hatano, H. Ikuta, R. K. Singh, N. Newman, and D. C. Larbalestier, "Effect of α-particle irradiation on a NdFeAs(O,F) thin film," Supercond. Sci. Technol. **31**, 034002 (2018).

[57] M. Eisterer, "Radiation effects on iron-based superconductors," Supercond. Sci. Technol. **31**, 013001 (2018).

[58] D. V. Efremov, M. M. Korshunov, O. V. Dolgov, A. A. Golubov, and P. J. Hirschfeld, "Disorder-induced transition between $s_\pm$ and s_{++} states in two-band superconductors," Phys. Rev. B **84**, 180512 (2011).

[59] C. Tarantini, M. Putti, A. Gurevich, Z. Shen, R. K. Singh, J. M. Rowell, N. Newman, D. C. Larbalestier, P. Cheng, Z. Jia, and H.-H. Wen, "Suppression of the critical temperature of superconducting NdFeAs(O,F) single crystals by Kondo-like defects sites induced by α-particle irradiation," Phys. Rev. Lett. **104**, 087002 (2010).

[60] R. Held, C. W. Schneider, J. Mannhart, L. F. Allard, K. L. More, and A. Goyal, "Low-angle grain boundaries in YBa$_2$Cu$_3$O$_{7-\delta}$ with high critical current densities," Phys. Rev. B **79**, 014515 (2009).

[61] T. Omura, T. Matsumoto, T. Hatano, K. Iida, and H. Ikuta, J. Phys.: Conf. Ser. **1054**, 012024 (2018).

[62] G. Deutscher, "Origin of weak-link behavior of grain boundaries in superconducting cuprates and pnictides," Appl. Phys. Lett. **96**, 122502 (2010).

[63] J. H. Durrell, C.-B. Eom, A. Gurevich, E. E. Hellstrom, C. Tarantini, A. Yamamoto, and D. C. Larbalestier, "The behavior of grain boundaries in the Fe-based superconductors," Rep. Prog. Phys. **74**, 124511 (2011).

[64] E. Sarnelli, M. Adamo, C. Nappi, V. Braccini, S. Kawale, E. Bellingeri, and C. Ferdeghini, "Properties of high-angle Fe(Se,Te) bicrystal grain boundary junctions," Appl. Phys. Lett. **104**, 162601 (2014).

[65] E. Sarnelli, C. Nappi, C. Camerlingo, E. Enrico, E. Bellingeri, S. Kawale, V. Braccini, A. Leveratto, and C. Ferdeghini, "Properties of Fe(Se,Te) bicrystal grain boundary junctions, SQUIDs, and nanostrips," IEEE Trans. Appl. Supercond. **27**, 7400104 (2017).

[66] E. Sarnelli, C. Nappi, A. Leveratto, E. Bellingeri, V. Braccini, and C. Ferdeghini, "Fe(Se,Te) superconducting quantum interference devices," Supercond. Sci. Technol. **30**, 065003 (2017).

[67] W. Si, C. Zhang, X. Shi, T. Ozaki, J. Jaroszynski, and Q. Li, "Grain boundary junctions of FeSe$_{0.5}$Te$_{0.5}$ thin films on SrTiO$_3$ bi-crystal substrates," Appl. Phys. Lett. **106**, 032602 (2015).

[68] S. Lee, J. Jiang, J. D. Weiss, C. M. Folkman, C. W. Bark, C. Tarantini, A. Xu, D. Abraimov, A. Polyanskii, C. T. Nelson, Y. Zhang, S. H. Baek, H. W. Jang, A. Yamamoto, F. Kametani, X. Q. Pan, E. E. Hellstrom, A. Gurevich, C. B. Eom, and D. C. Larbalestier, "Weak-link behavior of grain boundaries in superconducting Ba(Fe$_{1-x}$Co$_x$)$_2$As$_2$ bicrystals," Appl. Phys. Lett. **95**, 212505 (2009).

[69] S. Schmidt, S. Döring, F. Schmidl, V. Tympel, S. Haindl, K. Iida, F. Kurth, B. Holzapfel, and P. Seidel, "Bicrystalline grain boundary and hybrid SNS junctions based on Ba-122 thin films," IEEE Trans. Appl. Supercond. **23**, 7300104 (2013).

[70] T. Katase, Y. Ishimaru, A. Tsukamoto, H. Hiramatsu, T. Kamiya, K. Tanabe, and H. Hosono, "Advantageous grain boundaries in iron pnictide superconductors," Nat. Commun. **2**, 409 (2011).

[71] H. Hiramatsu, T. Katase, Y. Ishimaru, A. Tsukamoto, T. Kamiya, K. Tanabe, and H. Hoson, "Microstructure and transport properties of, [001]-tilt bicrystal grain boundaries in iron pnictide superconductor cobalt-doped BaFe$_2$As$_2$," Mater. Sci. Eng., B **177**, 515–519 (2012).

[72] K. Iida, S. Haindl, F. Kurth, J. Hänisch, L. Schultz, and B. Holzapfel, "BaFe$_2$As$_2$/Fe bilayers with, [001]-tilt grain boundary on MgO and SrTiO$_3$ bicrystal substrates," Phys. Procedia **45**, 189–192 (2013).

[73] T. Katase, Y. Ishimaru, A. Tsukamoto, H. Hiramatsu, T. Kamiya, K. Tanabe, and H. Hosono, "Josephson junction in cobalt-doped BaFe$_2$As$_2$ epitaxial thin films on (La,Sr)(Al,Ta)O$_3$ bicrystal substrates," Appl. Phys. Lett. **96**, 142507 (2010).

[74] T. Katase, Y. Ishimaru, A. Tsukamoto, H. Hiramatsu, T. Kamiya, K. Tanabe, and H. Hosono, "DC superconducting quantum interference devices fabricated using bicrystal grain boundary junctions in Co-doped BaFe$_2$As$_2$ epitaxial films," Supercond. Sci. Technol. **23**, 082001 (2010).

[75] S. Schmidt, S. Döring, F. Schmidl, F. Kurth, K. Iida, B. Holzapfel, T. Kawaguchi, Y. Mori, H. Ikuta, and P. Seidel, "Bicrystalline grain boundary junctions of Co-doped and P-doped Ba-122 thin films," J. Phys.: Conf. Ser. **507**, 012046 (2014).

[76] P. Seidel, "Josephson effects in iron based superconductors," Supercond. Sci. Technol. **24**, 043001 (2011).

[77] Y.-J. Kim, J. D. Weiss, E. E. Hellstrom, D. C. Larbalestier, and D. N. Seidman, "Evidence for composition variations and impurity segregation at grain boundaries in high current-density polycrystalline K- and Co-doped BaFe$_2$As$_2$ superconductors," Appl. Phys. Lett. **105**, 162604 (2014).

[78]J. D. Weiss, C. Tarantini, J. Jiang, F. Kametani, A. A. Polyanskii, D. C. Larbalestier, and E. E. Hellstrom, "High intergrain critical current density in fine-grain $(Ba_{0.6}K_{0.4})Fe_2As_2$ wires and bulks," Nat. Mater. **11**, 682–685 (2012).

[79]J. D. Weiss, A. Yamamoto, A. A. Polyanskii, R. B. Richardson, D. C. Larbalestier, and E. E. Hellstrom, "Demonstration of an iron-pnictide bulk superconducting magnet capable of trapping over 1 T," Supercond. Sci. Technol. **28**, 112001 (2015).

[80]Q. Zhang, H. Lin, P. Yuan, X. Zhang, C. Yao, D. Wang, C. Dong, Y. Ma, S. Awaji, and K. Watanabe, "Low-temperature synthesis to achieve high critical current density and avoid a reaction layer in $SmFeAsO_{1−x}F_x$ superconducting tapes," Supercond. Sci. Technol. **28**, 105005 (2015).

[81]H. Hilgenkamp and J. Mannhart, "Grain boundaries in high–T_c superconductors," Rev. Mod. Phys. **74**, 485–549 (2002).

[82]S. Graser, P. J. Hirschfeld, T. Kopp, R. Gutser, B. M. Andersen, and J. Mannhart, "How grain boundaries limit supercurrents in high-temperature superconductors," Nat. Phys. **6**, 609–614 (2010).

[83]H. Sato, H. Hiramatsu, T. Kamiya, and H. Hosono, "Enhanced critical-current in P-doped $BaFe_2As_2$ thin films on metal substrates arising from poorly aligned grain boundaries," Sci. Rep. **6**, 36828 (2016).

[84]K. Iida, H. Sato, C. Tarantini, J. Hänisch, J. Jaroszynski, H. Hiramatsu, B. Holzapfel, and H. Hosono, "High-field transport properties of a P-doped $BaFe_2As_2$ film on technical substrate," Sci. Rep. **7**, 39951 (2017).

[85]S.-W. Chan, "Nature of grain boundaries as related to critical currents in superconducting $YBa_2Cu_3O_{7−x}$," J. Phys. Chem. Solids **55**, 1415–1432 (1994).

[86]G. Hammerl, A. Schmehl, R. R. Schultz, B. Götz, H. Bielefeldt, C. W. Schneider, H. Hilgenkamp, and J. Mannhart, "Enhanced supercurrent density in polycrystalline $YBa_2Cu_3O_{7−\delta}$ at 77 K from calcium doping grain boundaries," Nature **407**, 162–164 (2000).

[87]X. Song, G. Daniels, D. M. Feldmann, A. Gurevich, and D. C. Larbalestier, "Electromagnetic, atomic structure and chemistry changes induced by Ca-doping of low-angle $YBa_2Cu_3O_{7−\delta}$ grain boundaries," Nat. Mater. **4**, 470–475 (2005).

[88]W. Si, J. Zhou, Q. Jie, I. Dimitrov, V. Solovyov, P. D. Johnston, J. Jaroszynski, V. Matias, C. Sheehan, and Q. Li, "Iron-chalcogenide $FeSe_{0.5}Te_{0.5}$ coated superconducting tapes for high field applications," Appl. Phys. Lett. **98**, 262509 (2011).

[89]W. Si, S. J. Han, X. Shi, S. N. Ehrlich, J. Jaroszynski, A. Goyal, and Q. Li, "High current superconductivity in $FeSe_{0.5}Te_{0.5}$-coated conductors at 30 Tesla," Nat. Commun. **4**, 1347 (2013).

[90]Z. Xu, P. Yuan, Y. Ma, and C. Cai, "High-performance $FeSe_{0.5}Te_{0.5}$ thin films fabricated on less-well-textured flexible coated conductor templates," Supercond. Sci. Technol. **30**, 035003 (2017).

[91]V. Braccini, "Fe(Se,Te) epitaxial thin films deposited on flexible metallic substrates," in Proceedings of 13th Biennial European Conference on Applied Superconductivity, EUCAS, Geneva, Switzerland (2017).

[92]S. Demura, M. Tanaka, A. Yamashita, S. J. Denholme, H. Okazaki, M. Fujioka, T. Yamaguchi, H. Takeya, K. Iida, B. Holzapfel, H. Sakata, and Y. Takano, "Electrochemical deposition of FeSe on RABiTS tapes," J. Phys. Soc. Jpn. **85**, 015001 (2016).

[93]A. Yamashita, R. Matsumoto, M. Tanaka, H. Hara, K. Iida, B. Holzapfel, H. Takeya, and Y. Takano, "Observation of zero resistance in as-electrodeposited FeSe," Solid State Commun. **270**, 72–75 (2018).

[94]K. Iida, J. Hänisch, S. Trommler, V. Matias, S. Haindl, F. Kurth, I. L. del Pozo, R. Hühne, M. Kidszun, J. Engelmann, L. Schultz, and B. Holzapfel, "Epitaxial growth of superconducting $Ba(Fe_{1−x}Co_x)_2As_2$ thin films on technical ion beam assisted deposition MgO substrates," Appl. Phys. Express **4**, 013103 (2011).

[95]S. Trommler, J. Hänisch, V. Matias, R. Hühne, E. Reich, K. Iida, S. Haindl, L. Schultz, and B. Holzapfel, "Architecture, microstructure and J_c anisotropy of highly oriented biaxially textured Co-doped $BaFe_2As_2$ on Fe/IBAD-MgO-buffered metal tapes," Supercond. Sci. Technol. **25**, 084019 (2012).

[96]T. Katase, H. Hiramatsu, V. Matias, C. Sheehan, Y. Ishimaru, T. Kamiya, K. Tanabe, and H. Hosono, "Biaxially textured cobalt-doped $BaFe_2As_2$ films with high critical current density over 1 MA/cm^2 on MgO-buffered metal-tape flexible substrates," Appl. Phys. Lett. **98**, 242510 (2011).

[97]Z. Xu, P. Yuan, F. Fan, Y. Chen, and Y. Ma, "Transport properties and pinning analysis for Co-doped $BaFe_2As_2$ thin films on metal tapes," Supercond. Sci. Technol. **31**, 055001 (2018).

[98]K. Iida, F. Kurth, M. Chihara, N. Sumiya, V. Grinenko, A. Ichinose, I. Tsukada, J. Hänisch, V. Matias, T. Hatano, B. Holzapfel, and H. Ikuta, "Highly textured oxypnictide superconducting films on metal substrates," Appl. Phys. Lett. **105**, 172602 (2014).

[99]H. Huang, C. Yao, C. Dong, X. Zhang, D. Wang, Z. Cheng, J. Li, S. Awaji, H. Wen, and Y. Ma, "High transport current superconductivity in powder-in-tube $Ba_{0.6}K_{0.4}Fe_2As_2$ tapes at 27 T," Supercond. Sci. Technol. **31**, 015017 (2018).

[100]X. Zhang, H. Oguro, C. Yao, C. Dong, Z. Xu, D. Wang, S. Awaji, K. Watanabe, and Y. Ma, "Superconducting properties of 100-m class $Sr_{0.6}K_{0.4}Fe_2As_2$ tape and pancake coils superconducting tapes," IEEE Trans. Appl. Supercond. **27**, 7300705 (2017).

[101]D. Dew-Hughes, "Flux pinning mechanism in type II superconductors," Philos. Mag. **30**, 293–305 (1974).

[102]P. Paturi, M. Malmivirta, H. Palonen, and H. Huhtinen, "Dopant diameter dependence of $J_c(B)$ in doped YBCO films," IEEE Trans. Appl. Supercond. **26**, 8000705 (2016).

[103]Q. Zhang, X. Zhang, C. Yao, H. Huang, D. Wang, C. Dong, Y. Ma, H. Ogino, and S. Awaji, "Enhanced transport current density in Sn-doped $SmFeAsO_{1−x}F_x$ tapes prepared by the PIT method," Supercond. Sci. Technol. **30**, 065004 (2017).

[104]S. C. Wimbush, *Flux Pinning in Applied Superconductivity Handbook on Devices and Applications* (WILEY, 2015), Chap. 1, pp. 85–87.

[105]R. Prozorov, M. A. Tanatar, R. T. Gordon, C. Martin, H. Kim, V. G. Kogan, N. Ni, M. E. Tillman, S. K. Bud'ko, and P. C. Canfield, "Anisotropic London penetration depth and superfluid density in single crystals of iron-based pnictide superconductors," Phys. C **469**, 582–589 (2009).